Turbulent Flow Modification in the Atmospheric Surface Layer over a Dense City

Lan Yao[1,2], Chun-Ho Liu[1,*], Guy P. Brasseur[3,4,5] and Christopher Y.H. Chao[6,7]

[1]Department of Mechanical Engineering, The University of Hong Kong, Hong Kong

[2]Thrust of Sustainable Energy and Environment, The Hong Kong University of Science and Technology (Guangzhou), Guangzhou, China

[3]Department of Civil and Environmental Engineering, The Hong Kong Polytechnic University, Hung Hom, Kowloon, Hong Kong

[4]Max Planck Institute for Meteorology, Hamburg, Germany

[5]National Center for Atmospheric Research, Boulder, Colorado, USA

[6]Department of Building Environment and Energy Engineering, The Hong Kong Polytechnic University, Hung Hom, Kowloon, Hong Kong

[7]Department of Mechanical Engineering, The Hong Kong Polytechnic University, Hung Hom, Kowloon, Hong Kong

Ref. No.: STOTEN-D-23-20975
Revised Manuscript Submitted
to
Science of the Total Environment
on
October 31, 2023

**Corresponding author address:*
Chun-Ho LIU
Department of Mechanical Engineering
7/F, Haking Wong Building
The University of Hong Kong
Pokfulam Road, Hong Kong
CHINA

Tel: +852 3917 7901 / +852 9788 7951
Fax: +852 2858 5415
Email: liuchunho@graduate.hku.hk
https://aplhk.tech
ORCID: 0000-0002-4609-524X

Graphical Abstract

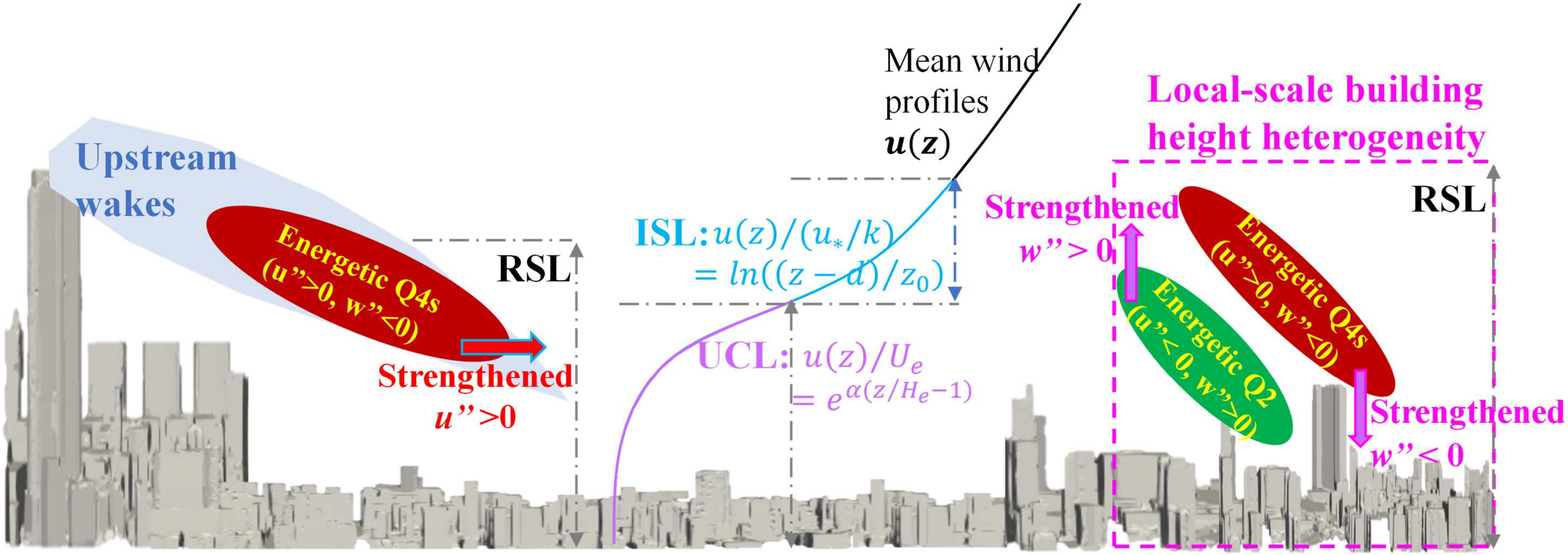

Highlights:

1. First parameterization of the RSL mean winds over a real city by exponential law
2. Specifications of the majority and intermittency of RSL winds
3. Physical evidence of zero-plane displacement as the drag center of ASL flows
4. Windy RSL does not necessarily imply favorable street-level winds and ventilation
5. Comparison of the roles of upstream wake and urban morphology in ASL flow dynamics

Turbulent Flow Modification in the Atmospheric Surface Layer over a Dense City

Lan Yao[1,2], Chun-Ho Liu[1], Guy P. Brasseur[3,4,5] and Christopher Y.H. Chao[6,7]

[1]Department of Mechanical Engineering, The University of Hong Kong, Hong Kong

[2]Thrust of Sustainable Energy and Environment, The Hong Kong University of Science and Technology (Guangzhou), Guangzhou, China

[3]Department of Civil and Environmental Engineering, The Hong Kong Polytechnic University, Hung Hom, Kowloon, Hong Kong

[4]Max Planck Institute for Meteorology, Hamburg, Germany

[5]National Center for Atmospheric Research, Boulder, Colorado, USA

[6]Department of Building Environment and Energy Engineering, The Hong Kong Polytechnic University, Hung Hom, Kowloon, Hong Kong

[7]Department of Mechanical Engineering, The Hong Kong Polytechnic University, Hung Hom, Kowloon, Hong Kong

Abstract

Winds in the atmospheric surface layer (ASL) over distinctive urban morphology are investigated by building-resolved large-eddy simulation (LES). The exponential law is applied to urban canopy layers (UCLs) unprecedentedly to parameterize vertical profiles of mean-wind-speed $\left.\langle\overline{u}\rangle\right|_z$ and examine the influence of morphological factors. The skewness of streamwise velocity S_u is peaked at the zero-plane displacement d (drag center) where flows decelerate mostly. The dynamics and intermittency in roughness sublayers (RSLs) are further contrasted. It helps determine the critical strength of the organized structures (ejection, Q2 and sweep (Q4) in their contributions to the average momentum transport (i.e., 3 $u''w''$ to 5 $u''w''$). Two key factors of the local-scale dynamics are revealed - building heterogeneity and upstream giant wakes that could amplify turbulence kinetic energy (TKE) and energetic intermittent Q4 by different mechanisms. The former is conductive for large-eddy generation that promotes vertical fluctuating velocity w'', stimulating intermittent, energetic Q2 and Q4. The latter, whose footprints are identified by the two-point correlation of streamwise velocity R_{uu} with specific size and inclination, facilitates intermittent, fast streamwise fluctuating velocity u'', forming vigorous Q4. Nevertheless, excessive planar density λ_p (≈ 0.7) is detrimental to both transport processes. These findings contribute to the theoretical and empirical wall models of large-scale roughness that help urban planners and policymakers to improve air quality.

Word count: 215

Keywords: atmospheric surface layer (ASL); wind parameterization; urban morphology; wake effect; turbulence structure; and urban canopy layer (UCL)

1. Introduction

Atmospheric-surface-layer (ASL) flows over dense cities are much more complicated than those over schematic layouts of idealized roughness elements commonly used in literature (Li & Bou-Zeid, 2019; Cheng & Yang, 2022). Topography configurations complicate the meteorological conditions, such as wind speed and direction, which govern the transport of inhalable particles and toxic gases (Guo et al., 2019; Zhao et al., 2021), together with the (aged and fresh) air exchange for urban aggregations. Hence, their in-depth understanding helps refine architectural design and urban planning for the management of accidental release and air quality, safeguarding the public health (Capolongo et al., 2020).

Identification of the key factors for bulk-flow properties over real urban setting is vital to elucidate turbulence dynamics, mixing processes, and pollutant dispersion (Palusci et al., 2022). Quantitative measures for wind parameterization, aerodynamic resistance, and turbulence characteristics are crucial to the pedestrian-level environment (Li et al., 2022; Liu et al., 2023). Especially, how ASL flows respond to urban morphology is important to practitioners, policymakers, and scientists working in environmental engineering and urban sustainability. This paper is thriving to approach these issues by calculating the winds over the downtown area of a megacity adopting building-resolved large-eddy simulation (LES).

Flows separate at building edges and the subsequent vortex shedding is crucial for pollutant removal (updraft) and fresh air entrainment (downdraft; Lim et al., 2022). In the recirculation behind buildings ($2H \leq x \leq 6H$; where x is the streamwise distance after the buildings and H the average building height; Peterka et al., 1985), shrank eddies suppress turbulence kinetic energy (TKE) over shorter blockages ($\leq H$ in this study) that weakens the ventilation in urban canopy layers (UCLs; Hertwig et al., 2019). The stagnant airflows would also worsen pollutant accumulation (Yuan et al., 2019). On the other hand, the wakes after high-rises would stimulate vortex shedding and strengthen updraft, facilitating pollutant removal (Han et al., 2017). It has also been shown that building downwash improves pedestrian-level winds (Letzel et al., 2012; Miao et al., 2014). Whereas, quantitative investigations into the roles of wakes in street-level air quality are limited.

Unlike a single, isolated building being considered in conventional wind engineering, the wakes after building clusters are giant, often extending a few kilometers downstream (Byrne et al., 2021; García-Sánchez et al., 2018; Hayati et al., 2019). The winds and turbulence are modified substantially, which, however, are rarely reported (Hertwig et al., 2019). The wakes after high-rise building clusters complicate the subsequent flows and transport. Analogously, the low-rises downstream could break up large eddies (Lim et al., 2022). Unlike classic flow regimes (Oke, 1988), quantifying the interactions of the multiscale wakes generated by actual urban buildings are not yet available. Advanced understanding of microscale flow response to urban morphology, especially in dense cities, is therefore crucial.

Megacities are characterized by diversified building geometry. By schematic layouts of cuboids, it has been shown that the maximum H_{max} and standard deviation σ_{Ha} of building height are crucial to the dynamics. The friction velocity u_τ and the zero-plane displacement d depend more tightly on H_{max} rather than H (Sützl et al., 2020). Buildings with $\sigma_{Ha} \geq 0.4H$ could reduce pollutant concentrations by 70% (Papp et al., 2021). Real urban areas feature more complicated, heterogeneous buildings. For example, σ_{Ha} is up to H in Los Angeles (Ratti et al., 2002) and Abu Dhabi (Ramirez et al., 2018) but the influence on ASL winds is unknown. Moreover, σ_{Ha} of schematic layouts is much smaller (say H; Huang et al., 2021) than that of megacities. For instance, the existence of skyscrapers in street or neighborhood scales soars σ_{Ha} to $10H$ for Seoul (Park, Baik, & Lee, 2015) or even $12H$ for Tokyo (Kanda et al., 2013). It is recognized that horseshoe vortices are important to coherent structures and large-scale streaks (Adrian et al., 2000). However, those around skyscrapers ($h \geq 100$ m; Drobinski et al., 2004) may not sustain but entrain into the legs of the leeward arch vortices (Yakhot et al., 2006). How the excessively heterogeneous urban surfaces affect the turbulence generation, coherent structures, and turbulence statistics, is not available yet.

The complexity of winds over urban areas is the major issue for parametrization, especially in the roughness sublayers (RSLs) close to buildings. The exponential law (exp-law) has been tested over urban-like rough surfaces (Li & Katul, 2022). It was initially derived for vegetation canopies in which the mixing length and the drag coefficient were assumed constant (Cionco, 1965). Whereas, it is not the case for urban areas (Castro, 2017). Extending the exp-law to urban-like roughness is acknowledged by their similar (inflected) RSL/UCL mean-wind-speed (MWS) profiles based on the plane-mixing-layer theory (Yang et al., 2016). The reliability of this extension, however, is debatable because of urban heterogeneity. The applicability of the exp-law to RSL/UCL flows over real urban morphology remains an open question.

Other than those based on vortex method and Green's function (Furtak-Cole & Ngan, 2020), most RSL MWS parametrizations are the variants of Monin-Obukhov similarity theory (MOST; Harman & Finnigan, 2007). Although they predicted well the RSL winds over dense cities, there exists a natural defect that the ASL is displaced upward (d; Ho & Liu, 2017). The flows below that plane is however unavailable. Especially, the zero-plane displacement of real cities ($1.2H \leq d \leq 3.6H$) is much higher than that reported of uniform cuboids ($0.8H$; Coceal et al., 2007). The winds in the vicinity of buildings are core ASL dynamics which can merely be addressed by the conventional approach unfortunately.

This paper focuses on the LES of a dense city, Hong Kong. The numerical method and building information are detailed in Sec. 2. The mean and turbulence properties are reported in Sec. 3 which is further partitioned into: MWS parameterizations (Sec. 3.1); momentum transport and turbulence strength (Sec. 3.2); flow anisotropy in streamwise and vertical direction (Sec. 3.3); extremity and intermittency of velocity fluctuations (Sec. 3.4); quadrant analysis (Sec. 3.5); together with eddy structures (Sec.3.6). Sec. 4 discusses the practical implication of the results obtained. Sec. 5 concludes the findings and outcome.

2. Methodology

2.1 Numerical Method

LES is adopted in this paper whose mathematical model is detailed in Yao et al., (2022). In brief, the governing equations are decomposed into resolved-scale $\overline{\psi}$ and subgrid-scale (SGS) ψ' variables. The Smagorinsky model (Smagorinsky, 1963) and the SGS TKE conservation (Li et al., 2008) are employed for SGS parameterization. The finite volume (FV) method is used for spatial discretization. The velocity-pressure coupling in incompressible flows is solved by the combination of pressure implicit with splitting of operator (PISO) and semi-implicit method for pressure-linked equations (SIMPLE). The cell-limited gradient and limited linear divergence schemes are used, respectively, to calculate the gradient and divergence terms. The first-order-accurate, implicit Euler scheme is used for time integration.

The current LES was validated by wind tunnel experiments elsewhere (Cheng & Yang, 2022; Mo and Liu, 2023). Selected vertical profiles of mean and turbulence statistics were compared well. The mild discrepancies are attributed to the inherent differences between laboratory experiments and mathematical models, such as inevitable errors caused by instrumentation, fabrication of physical models, approximation to numerical methods, dissimilar background turbulence levels, or empirical modeling constants. Nevertheless, our LES is capable of calculating the flows over a real city with diversified urban morphology.

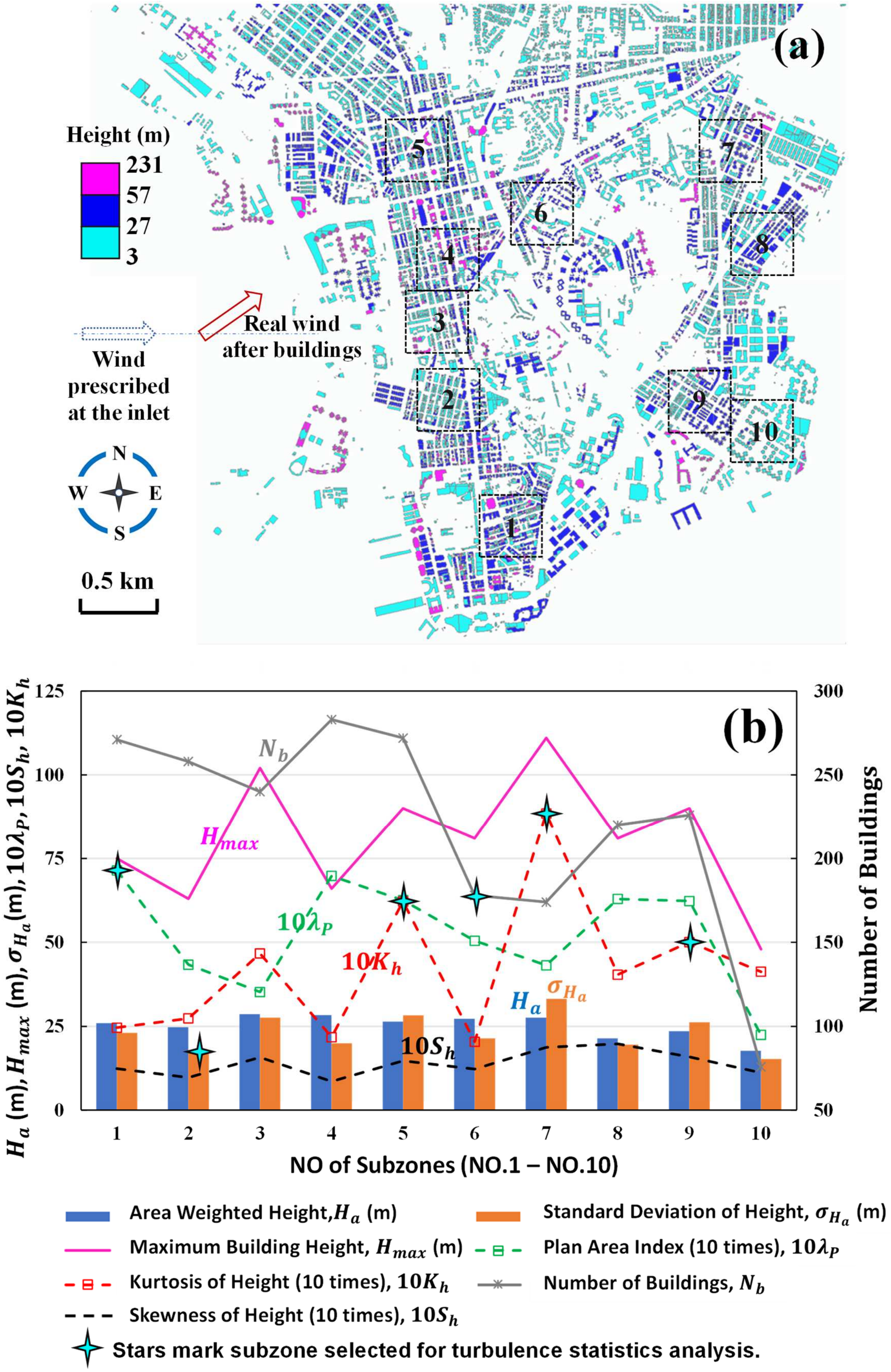

Figure 1. (a) Building height distribution in Kowloon Peninsula, Hong Kong and the ten subzones (dashed squares). (b) Building statistics and urban configuration.

2.2 Model Setup

Kowloon Peninsula, Hong Kong (downtown area 4.4 × 4.4 km^2) is digitalized in which the buildings are resolved explicitly (data source: the Survey and Mapping Office of Lands Department, HKSAR Government). The computation domain sizes 10 km (east-west) × 13 km (south-north) × 1 km (vertical; z) that is discretized into 11 million FV hexahedra. A background pressure gradient is prescribed such that the freestream wind speed U_∞ is around 10 m sec^{-1} from the Southwest. The Reynolds number Re (= $U_\infty H_{max}/\nu$; where H_{max} = 490 m is the height of the tallest building and $\nu = 1.56 \times 10^{-5}$ m^2 sec^{-1} the kinematic viscosity of air) is over 10^8 so the turbulent flows are full-developed (Elbing et al., 2011).

Five morphological indicators are used to quantify the surface topology in terms of the building density and the height distribution. The plan area index

$$\lambda_p = \frac{A_p}{A_l} = \sum_{i=1}^{N_b} \frac{A_i}{A_l} \tag{1}$$

measures the building density where A_p is the sum of the projected area of individual buildings A_i and N_b the number of buildings in a subzone. Real urban morphology is composed of buildings with diversified sizes, shapes, and orientation. The building volume is utmost important to the UCL flows. In this connection, the area-weighted building height

$$H_a = \frac{\sum_{i=1}^{N_b} h_i \times A_i}{\sum_{i=1}^{N_b} A_i} \tag{2}$$

is adopted to compare the subzone blockage where h_i is the height of building i. Besides, the standard deviation

$$\sigma_{Ha} = \sqrt{\sum_{i=1}^{N_b} \left(h_i - H_a\right)^2 \Big/ N_b} \tag{3}$$

and the skewness

$$S_h = \frac{\sum_{i=1}^{N_b} (h_i - H_a)^3 \Big/ N_b}{\sigma_{H_a}^3} \tag{4}$$

of building height are calculated to characterize the urban morphology of the ten selected subzones (Figure 1b). Previous studies demonstrated the significance of high-rises to ASL flows (Xie & Castro, 2009). Hence, the kurtosis of building height

$$K_h = \frac{\sum_{i=1}^{N_b} (h_i - H_a)^4 \Big/ N_b}{\sigma_{Ha}^4} \tag{5}$$

is included to account for the (minor) high-rises in building-height heterogeneity.

To reveal the mechanisms of turbulence dynamics in the ASL flows over dense urban areas with large spatial heterogeneity in megacities, e.g., Los Angeles ($\lambda_p \approx 0.28$, $\sigma_{Ha} \approx H_a$) (Ratti et al., 2002) and Tokyo ($\lambda_p \approx 0.4$, $\sigma_{Ha} \geq 0.65H_a$) (Yoshida et al., 2018), ten subzones (individual lot area $A_l = 0.4 \times 0.4$ km^2) across the downtown (Figure 1a) are selected. Their morphological features, such as substantial building height heterogeneity ($\sigma_{Ha}/H_a \geq 0.7$ for all the subzones and $K_h \geq 4$ for NO.3, NO.5, NO.7, NO.8, NO.9, and NO.10), are similar. The characteristic size of each subzone complies with that of neighborhood scale (0.2 km to 1 km) (Xu and Gao, 2022). It is a crucial parameter in urban environment, affecting street-level ventilation and urban heat island (Sabatino et al., 2020; Britter and Hanna, 2003). The height of majority buildings is in the range of 3 m $\leq h \leq$ 27 m (Figure 1a) and the area-weighted building height H_a is around 25 m (Figure 1b). To the southwest of the subzones NO.2 and NO.5, there exist several high-rise building clusters ($h \geq 150$ m) that initiate giant wakes over the downtown in Southwesterly winds (Appendix, Figure A1). The main streets (most are South-North oriented) cross all the subzones. A vast number of buildings are erected in the commercial districts (subzones NO.1 to NO.5). Especially, the subzones NO.1 and NO.4 are densely built ($\lambda_p = 0.71$ and $N_b \geq 270$). A large number of slender buildings with relatively uniform height ($\lambda_p = 0.43$, $N_b = 258$, and $\sigma_{Ha} = 0.72H_a$) are sparsely distributed in NO.2. On the contrary, uniform-height, bulky buildings ($\lambda_p = 0.5$, $N_b = 178$, and $\sigma_{Ha} = 0.78H_a$) reside in NO.6. Most of the buildings in the subzones NO.3, NO.5, NO.7, and NO.9 are tall ($H_{max} \geq 3.4H_a$) that possess wide spectra of height distribution ($\sigma_{Ha} \geq H_a$ and $K_h \geq 5$). Among others, the tallest building of the entire computation domain is in NO.7 ($H_{max} = 4H_a$) where the buildings are sparse such that the kurtosis of building height is as high as $K_h = 9$.

In the sake of distinct geometric features, 6 out of 10 subzones (NO.1, NO.2, NO.5, NO.6, NO.7, and NO.9) are further analyzed for turbulence statistics in Sec. 3.2 to Sec. 3.5. Apart from the most densely built NO.1, there are three high-K_h subzones (NO.5, NO.7, and NO.9) and another two with rather uniform building height (NO.2: slender buildings and NO.6: bulky, $0.72 \leq \sigma_{Ha}/H_a \leq 0.78$). Hereafter, the statistics are presented as ensemble (both time- and horizontal-plane) average of individual subzones $<\psi>$ and fluctuation ψ'' (= ψ - $<\psi>$) at different vertical levels z.

3. Results

3.1 RSL Identification

The log-law

$$\left\langle \overline{u} \right\rangle \Big|_z = \frac{u_\tau}{\kappa} \times \ln\left(\frac{z-d}{z_0}\right) \tag{6}$$

is applied to the LES-calculated inertial sublayer (ISL) MWS profile of each subzone (Figure 2 and Figure A2 in Appendix). Here, κ (= 0.42) is the von Kármán constant. The friction velocity u_τ (= $<- u''w''>_{\max}^{1/2}$) is determined by the maximum downward momentum flux (Yao et al., 2022). The aerodynamic parameters of the log-law (zero-plane displacement d and roughness length z_0) as well as the RSL height z^* (i.e., ISL bottom) are then determined by linear regression (Table A1 in Appendix).

Results show that a longer z_0 tends to manifest a rougher urban area that is in line with (stronger) u_τ (Table A1 in Appendix). It in turn corroborates the applicability of the conventional turbulent boundary layer (TBL) theory over a smooth wall to a rough wall. Other than NO.2 and NO.5, the LES-calculated z^* ($\approx 4H_a$) agrees well with that available in literatures ($3H_a \leq z^* \leq 5H_a$; Zhu et al., 2017). The elevated RSLs observed in the subzones NO.2 and NO.5 (almost $5H_a \leq z^* \leq 6H_a$; 20% higher) could be attributed to the giant wakes after the building clusters to the Southwest (Figure 1a and Figure A1 in Appendix). The winds interact with the distinctive high-rises in NO.2 ($H_{max} = 2.5H_a$) and NO.5 ($H_{max} = 3.6H_a$) that raises the inhomogeneous RSL eventually.

3.2 UCL MWS Profiles

The wind typically inflects uniformly at the top of vegetation (Luhar et al., 2008) or building roof of idealized, homogeneous canopies (Sützl et al., 2020) which acts as an interface differentiating the dynamics below and above UCL (Xie et al., 2008). In a real city, however, it seldom inflects at z = H because of the heterogeneity (Giometto et al., 2016). The UCL height is therefore determined by the inflection (z = H_e) of MWS profile, which is located above the mean building height ($1.8 \leq H_e/H_a \leq 4.1$; Table A1 in Appendix). Although debatable, assuming constant drag coefficient C_d and mixing length l_m yields the following widely adopted exp-law of MWS profile

$$\left.\langle \bar{u} \rangle\right|_z = U_{H_e} \times \exp\left[\alpha \times \left(\frac{z}{H_e} - 1\right)\right] \qquad (7)$$

for urban setting (Castro, 2017). Here, U_{He} is the MWS at $z = H_e$ and α the attenuation coefficient in response to urban morphology (Böhm et al., 2013). Equation (7) transforms smoothly from the UCL upward to the ISL (log-law) via the inflection. The transport induced by spatial inhomogeneity, such as dispersive stress, is neglected in the equation, which, however, was found invalid in vegetation (Luhar et al., 2008) or urban (Santiago & Martilli,

2010) canopies. Besides, the UCL mixing length l_m is merely constant but exhibits a local maximum at $z = 0.5H_a$ (Cheng & Yang, 2022).

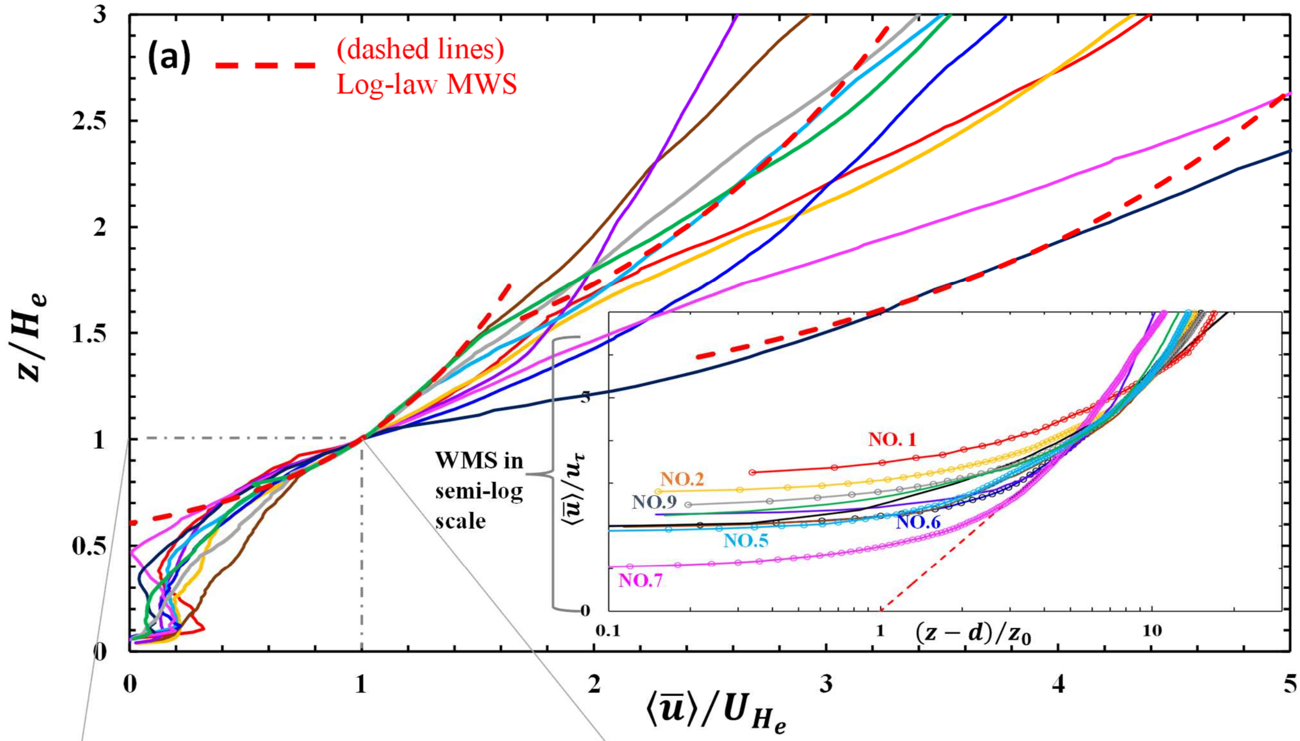

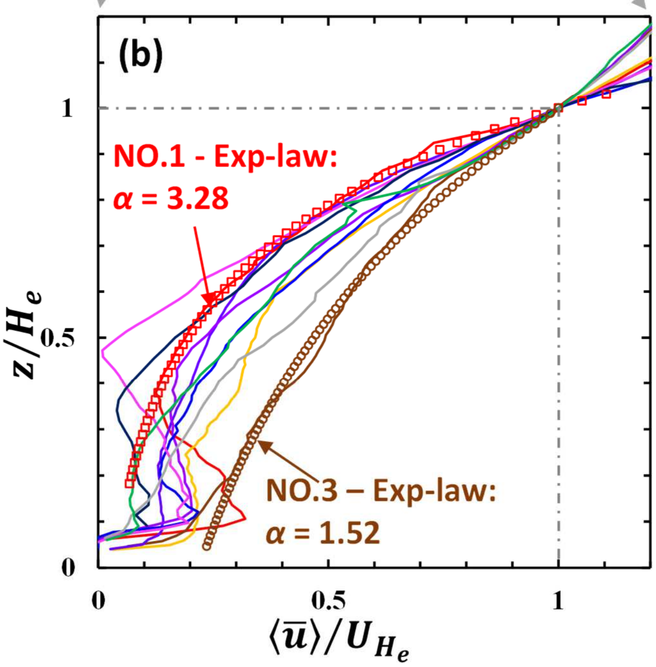

Subzone	H_e/H_a	α	ISL/H_e	MWS Symbol
NO. 1	2.64	3.28	1.33 - 1.62	red line
NO. 2	4.16	2.12	1.47 - 1.67	yellow line
NO. 3	3.48	1.52	1.06 - 1.44	brown line
NO. 4	3.64	2.90	0.74 - 0.85	purple line
NO. 5	2.80	2.53	2.14 - 2.68	light blue line
NO. 6	3.96	2.39	1.01 - 1.24	blue line
NO. 7	2.88	3.28	1.53 - 1.92	magenta line
NO. 8	1.96	3.25	1.70 - 2.11	black line
NO. 9	2.48	2.06	1.40 - 1.80	grey line
NO. 10	2.68	2.55	1.33 - 1.48	green line

Figure 2. (a) LES-calculated MWS profiles $\langle \overline{u} \rangle / U_{He}$ plotted against height z/H_e of the ten subzones. (b) Enlarged window with exponential fitting Equation (9) for subzones NO.1 (red squares; maximum $\alpha = 3.28$) and NO.3 (brown circles; minimum $\alpha = 1.52$).

Equation (7) was applied to idealized roughness elements (Cheng & Castro, 2002). An analytical model of MWS profile based on MOST was proposed by Mo et al. (2021) but it is intrinsically limited to the upper RSL above drag center $z > d$. Whereas, d could reach as high as $3H_a$ in sub-kilometer scale (Sützl et al., 2020) and even $4H_a$ for the building-resolved LES in this study. Under this circumstance, modeling the majority RSL flows could not be easily attained. Regardless of the spatial heterogeneity of real urban morphology, minimizing the root-mean-square errors between Equation (9) and the current LES-calculated MWS $\langle \overline{u} \rangle$ arrives attenuation α in response to urban morphology ($1.5 \leq \alpha \leq 3.3$; Figure 2 and Table A1 in Appendix).

The attenuation of all the UCL MWS profiles falls within 1.5 (NO.3) $\leq \alpha \leq$ 3.3 (NO.1, NO.7, and NO.8; Figure 2b and Table A1 in Appendix). A larger α signifies a faster diminishing RSL flow toward the UCL, and vice versa. It in turn results in a substantial difference in RSL and UCL wind speeds. Hence, a windy RSL does not necessarily imply favorable pedestrian-level ventilation that is probably attributed to building blockage and/or flank. The RSL/UCL winds in NO.3 diminish most slowly due to the "chopstick" architectural design, resulting in a small packing density ($N_b = 240$ and $\lambda_p = 0.35$). Compared with the real urban morphology in this study ($0.24 \leq \lambda_p \leq 0.71$), schematic layout is smoother in which the attenuation is even smaller. For example, the attenuation α equals 1.1 and 1.8 for aligned and staggered cases, respectively, with $\lambda_p = 0.25$ (Yang et al., 2016). Whereas, α does not exhibit a simple relationship to either momentum transport or aerodynamic resistance.

Although the subzones NO.3 ($u_\tau = 0.42$ m sec^{-1} and $\alpha = 1.5$) and NO.7 ($u_\tau = 0.54$ m sec^{-1} and $\alpha = 3.3$) are roughest, their UCL attenuation is very different. Similarly, schematic layouts with the same λ_p but different roughness would double the attenuation α, e.g. the cuboid cases

L11A and L25A in Yang et al., (2016). As shown in the current LES, the subzones with large α either have large λ_p (NO.1, NO.4 and NO.8) or substantial building height heterogeneity (elevated σ_{Ha} and K_h; NO.7). Hence, dense, heterogeneous urban areas slow down the UCL flows. In brief, the attenuation α of real urban areas is larger than that of the schematic ones. The plan area index (λ_p), building heterogeneity (σ_{Ha} and K_h), and road alignment could modify the UCL winds substantially.

Although the shear at the inflection $z = H_e$ is well represented by the exp-law Equation (7), previous results of urban-like roughness elements underestimated the attenuation α due to shear-layer thickening (Xie et al., 2008). A mild deviation from Equation (7) arises in this study due to the real-urban heterogeneity. For example, in the subzones NO.7 and NO.8, the mean-wind speeds for $z \leq 1.8H_a$ are merely described by the exp-law (Figure 2). Besides, pedestrian-level winds could be faster than the exp-law because of the flow channeling under certain incident angle (Castro, 2017). Close to the ground ($z \leq 0.05H_e$), recirculating winds (negative $\langle \overline{u} \rangle$; Figure 2) were reported elsewhere (Coceal et al., 2006). Large deviations from the exp-law are thus found within the bottom 20% to 25% of RSL (Yang et al., 2016) where the MWS drops sharply (Leonardi & Castro, 2010). In general, the exp-law could well predict the UCL MWS profiles ($z \leq H_e$), especially in the region where the log-law ($z \geq d$) fails since the inflection is above the zero-plane displacement ($0.69 \leq d/H_e \leq 0.99$; Table A1 in Appendix).

3.3 Momentum Transport and Turbulence Intensity

For a succinct representation, the results of 6 subzones (NO.1, NO.2, NO.5, NO.6, NO.7, and NO.9) scattering across the peninsula (Figure 1) are examined in the subsequent sections. Because of the dominated turbulence production, the vertical variations of streamwise fluctuating velocity $\langle u''u''\rangle^{1/2}/U_\infty$ and TKE are similar (Figure 3). In $4H_a \leq z \leq 5H_a$, TKE is either peaked (in NO.1, NO.6, and NO.9) or inflected (in NO.5 and NO.7). Specifically, the peak is located as high as $z \geq 6H_a$ in NO.2 (and NO.5) because of the wakes after the high-rises to the Southwest and the elevated zero-plane displacement ($d = 4H_a$). The wakes extend above subzones NO.2 and NO.5, amplifying the mixing layer. In addition, more pronounced u'' peaks are observed over the ISLs in subzones NO.5, NO.7, and NO.9 where the buildings are extremely heterogeneous ($K_h \geq 5$ and $\sigma_{Ha} \geq H_a$) whose maximum height exceeds 90 m ($3.6H_a$; Figure 1b). It is therefore suggested that pencil-like high-rises would modify the ASL flows downstream substantially (Hertwig et al., 2021). Obviously, the TKE in subzones NO.5 and NO.9 (both $\lambda_p = 0.62$) is more intensified than that in NO.7 ($\lambda_p = 0.43$). This is because more obstacles disturb the flows, triggering the turbulence aloft. Besides, the peaked streamwise fluctuating velocity is largest in NO.5 (Figure 3). As discussed previously, it would be the collective effect of wakes and building heterogeneity, including maximum building height H_{max}, plan area index λ_p, and building height standard deviation σ_{Ha}.

Other than NO.7, the maximum downward momentum flux $-\langle u''w''\rangle/U_\infty^2$ coincides with the strong shear (together with the maximum $\langle u''u''\rangle^{1/2}/U_\infty$). In NO.7, on the contrary, possesses the highest H_{max}, H_a, and σ_{Ha}, leading to a broad range of motion scales at elevated level ($7H_a \leq z \leq 11H_a$). It is speculated that, with heterogeneous buildings ($K_h \geq 3$ and $\sigma_{Ha} \geq H_a$), the aggregated wakes complicate the turbulence structure (e.g. NO.5 with maximum $\langle u''u''\rangle^{1/2}/U_\infty$) while the local, diversified building height variability (H_a, H_{max}, and σ_{Ha}) determine the transport (e.g. NO.7 with largest $-\langle u''w''\rangle/U_\infty^2$). Especially, high-rises ($h \geq 200$ m) possess non-negligible effects on wake dynamics (Cheng et al., 2021). On the other hand, in NO.1 with excessive λ_p (≈ 0.7), both the momentum flux and TKE are weakened because the skimming flows over idealized geometry seldom penetrate the canopy level (He et al., 2019). It is detrimental to turbulent transport, suppressing pedestrian-level winds.

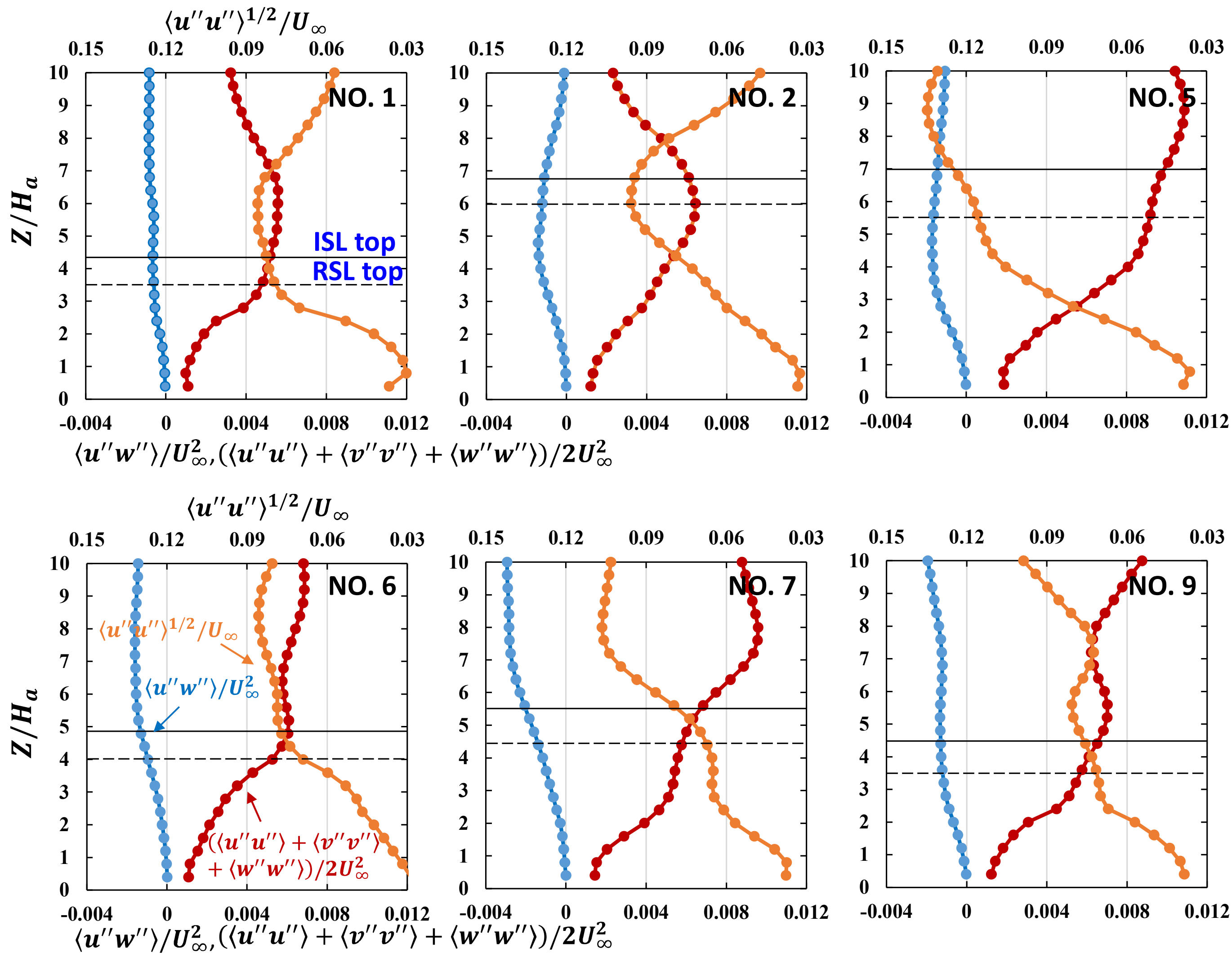

Figure 3. Momentum flux $<u''w''>/U_\infty^2$, TKE $(<u''u''> + <v''v''> + <w''w''>)/2U_\infty^2$, and streamwise fluctuating velocity $<u''u''>^{1/2}/U_\infty$ plotted as functions of height z/H_a.

3.4 Skewness and Kurtosis of Velocity

The skewness of RSL streamwise velocity S_u is positive (Figure 4), hence, the streamwise flow is skewed with rare, pronounced acceleration ($u'' >> 0$) and recurring, moderate deceleration ($u'' < 0$). The maximum S_u coincides with d in $2H_a \leq z \leq 4H_a$ (Table A1 in Appendix) so aerodynamic resistance acts like the driving force, leading to the RSL gusts commonly observed. Above its local maximum, S_u reduces, crosses zero then turns to negative. The zero-crossing is located around the RSL-ISL interface for NO.7 and NO.9, that is up in the

ISL for the rest subzones. In subzones NO.2 and NO.5, the elevated upstream wakes (discussed in Sec. 3.2) affect streamwise TKE that raise the positive S_u to higher elevation ($z \geq 7H_a$). Their broad ($2H_a \leq z \leq 4H_a$), large S_u (≈ 0.7) signifies the massive deceleration in the vicinity of drag center $z = d$ which is elevated above the peaked S_u in NO.2 resulting from the slow air masses encompassed in the giant upstream wakes.

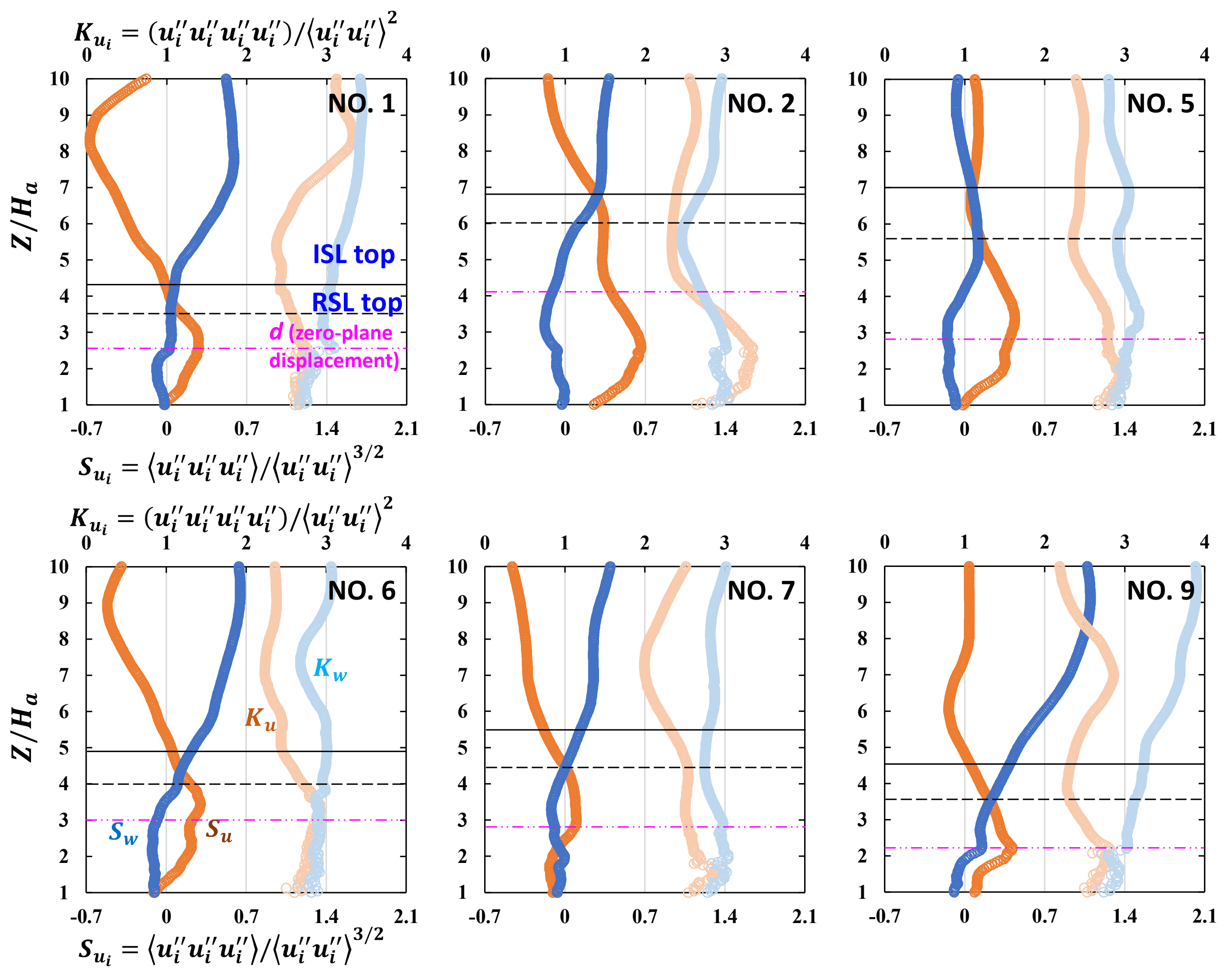

Figure 4. Skewness S_{ui} ($= \langle u_i'^3\rangle / \langle u_i'^2\rangle^{3/2}$) and kurtosis K_{ui} ($= \langle u_i'^4\rangle / \langle u_i'^2\rangle^2$) of streamwise u and vertical w velocities plotted as functions of height z/H_a.

Aside from NO.9, the skewness of RSL vertical velocity S_w is negative that switches to positive over the RSL-ISL interfaces (Figure 4). The negative S_w demonstrates that, from the ground level, most slow air masses are transported upwards ($w'' > 0$). On the other hand, the positive S_w at higher elevation signifies downdraft ($w'' < 0$). For rougher surfaces (subzones NO.2, NO.5 and NO.7), majority slow detrainment ($w'' > 0$ and $S_w < 0$) resides at higher elevation ($z > 4H_a$). However, for the less rough but densely built subzones (NO.1 and NO.9), most fast entrainment ($w'' < 0$ and $S_w > 0$) penetrates more deeply. In view of the height variability in NO.9, enhanced entrainment diagnoses its upper RSL by appreciable positive S_w.

Different from other subzones, the kurtosis $K_u < 3$ in NO.2 that embellishes the intermittent streamwise flows in the lower RSL. In our previous study, $K_u > 3$ was notable in the lower RSL because of a skyscraper ($h > 200$ m) nearby (Yao et al., 2022). A fraction of intermittent streamwise acceleration is likely induced by the wakes associated with neighboring high-rise buildings and urban roughness. This intermittency is intensified mostly (where K_u peak is gained) around the S_u peak in NO.2. Along with such deceleration, intermittent, extreme streamwise acceleration takes place around the drag centers $z = d$ of urban areas.

Generally, $S_u > 0$ and $S_w < 0$ in RSLs, hence, slower winds ($u'' \leq 0$) are ejected ($w'' \geq 0$). On the other hand, faster winds are entrained ($S_u < 0$ and $S_w > 0$) above RSL-ISL interface. Yet, $S_u > 0$ and $S_w > 0$ are found coexist in the ISLs in the subzones NO.2, NO.5, and NO.6, or in most RSL in NO.9. This part will be elaborated by conditional sampling in Sec 3.5. The vertical flows are not intermittent in most subzones ($K_w < 3$). However, $K_w > 3$ is notable in the ISL of NO.9 where a nonzero S_w is evident. This pair of nonzero S_w (S_u) and K_w (K_u) > 3 illustrate highly intermittent, ascending (accelerating) flows with elevated turbulence intensities, implying the potential contribution to the aged air removal from pedestrian level.

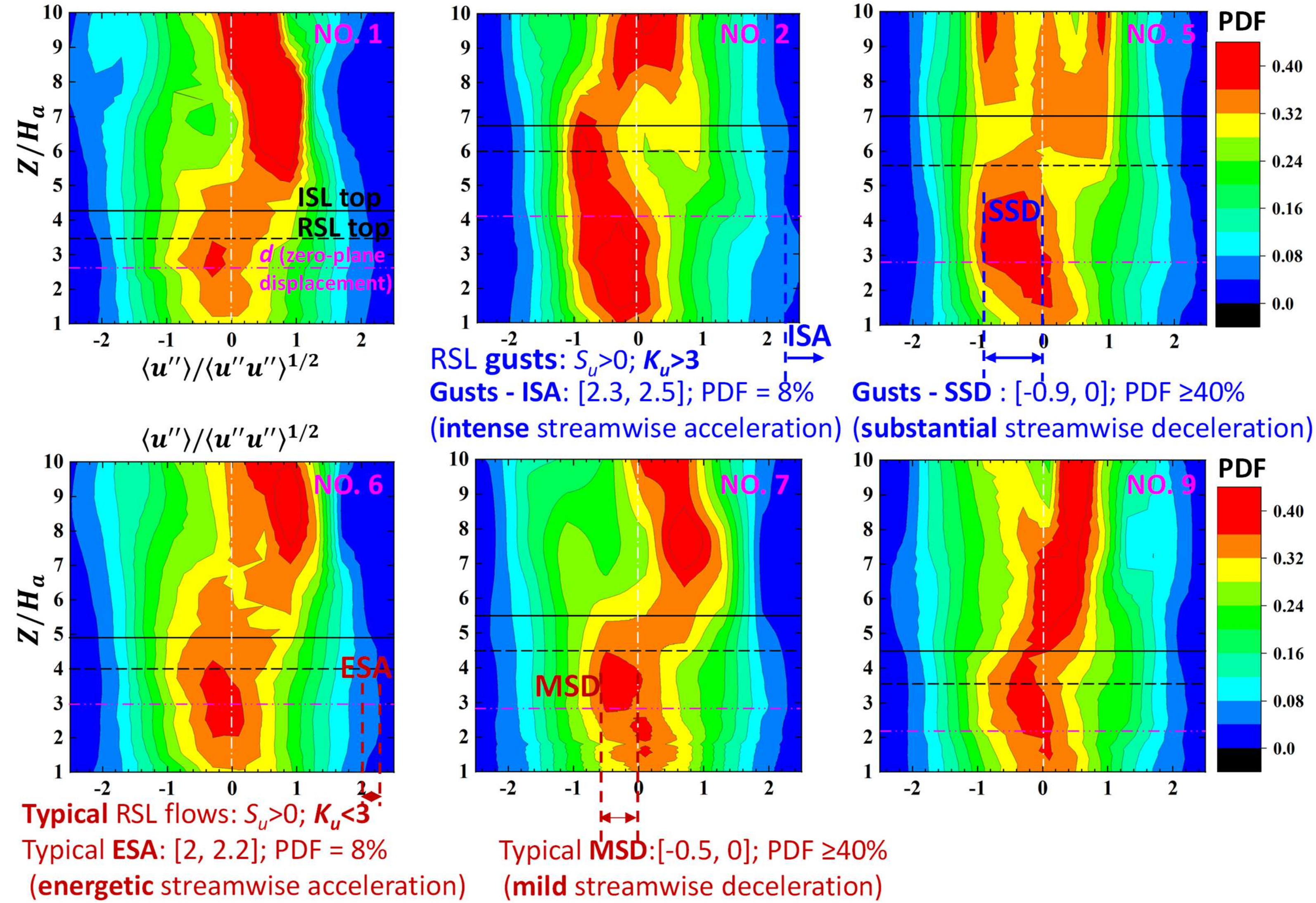

Figure 5. (a). Shaded contours of probability density function of streamwise fluctuating velocity $<u''>/<u''u''>^{1/2}$ at different elevation z/H_a.

3.5 Probability Density Function of Velocity Fluctuation

To differentiate the velocity fluctuations with a range of magnitude and occurrence (probability density function; PDF), RSL flows are divided based on the skewness and kurtosis (Figure 5 and Table A2 in Appendix).

The PDF of streamwise velocity is asymmetric (Figure 5a). Within the RSLs, on the left-hand side (LHS) of zero fluctuation, there is a high probability of mild streamwise deceleration (MSD; PDF($-0.5 \leq u''/\langle u''u''\rangle^{1/2} \leq 0$) ≥ 0.4), resulting in a positive RSL S_u. On the right-hand side (RHS), energetic streamwise acceleration (ESA) is more frequent (PDF($2 \leq u''/\langle u''u''\rangle^{1/2} \leq 2.2$) $= 0.08$) than its extreme deceleration counterpart. At the high-probability regime (PDF($u''/\langle u''u''\rangle^{1/2}$) ≥ 0.4), the contours shrink mostly on the LHS but expand towards strong accelerations ($u'' >> 0$) on the RHS. This exaggerates the difference between the major deceleration and minor acceleration, resulting in the maximum S_u.

In the subzones NO.2 and NO.5, the frequent, substantial streamwise deceleration (SSD; PDF($-0.9 \leq u''/\langle u''u''\rangle^{1/2} \leq 0$) $= 0.4$) leads to highly skewed RSL streamwise flows. Especially, major, much more biased streamwise decelerations ($-0.9 \leq u''/\langle u''u''\rangle^{1/2} \leq -0.6$), together with intense streamwise acceleration (ISA; PDF($2.3 \leq u''/\langle u''u''\rangle^{1/2} \leq 2.5$) $= 0.08$) appears more often in NO.2 than does in other subzones. The scarce and extreme portion diagnoses highly intermittent turbulent flows in NO.2. Moreover, the streamwise fluctuations are strong around the drag center $z = d$. For example, PDF($u''/\langle u''u''\rangle^{1/2} \geq 3$) ≥ 0.04 is observable (the threshold of gusty wind; Duan & Takemi, 2021).

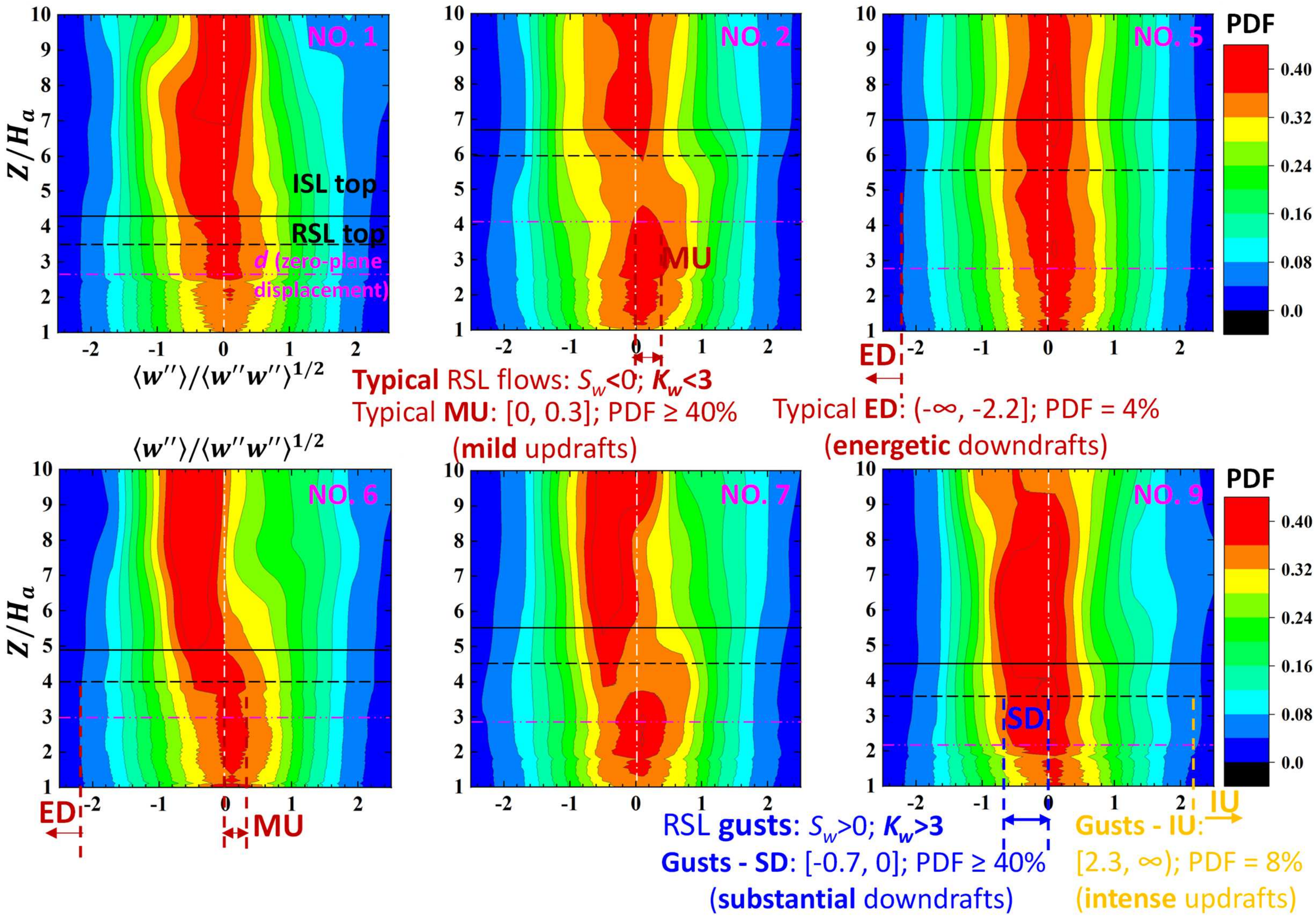

Figure 5. (b). Shaded contours of probability density function of vertical fluctuating velocity $<w''>/<w''w''>^{1/2}$ at different elevation z/H_a.

372

For the RSL vertical fluctuating velocity, the high-probability contours lean to the RHS (Figure 5b). The magnitude of the vertical fluctuating velocity (MU; $w''/<w''w''>^{1/2} = 0.3$) is slower than its streamwise counterpart (MSD; $u''/<u''u''>^{1/2} = -0.5$). Compared with the u'' contours, the w'' ones are more uniform that concur the smaller S_w magnitude (more symmetric PDF) and vertical variations explained in Sec. 3.3 (Figure 4). In line with the negative skewness, energetic RSL vertical fluctuating velocity tends to be downward (ED; PDF($w''/<w''w''>^{1/2} \leq -2.2$) = 0.04). Among all the subzones, the PDF of streamwise fluctuating velocity is most symmetric in NO.1 (Figure 5a). It is thus suggested that an exceptionally dense, built area ($\lambda_p \geq 0.7$) would suppress turbulence because of the dominated skimming flows.

Above elevation $z \geq 2H_a$ in NO.9, substantial downdraft appear frequently (SD; PDF($-0.7 \leq w''/<w''w''>^{1/2} \leq 0$) $\geq$ 0.4; Figure 5b). It provokes a large kurtosis ($K_w \geq 3$) together with intermittent, intense updraft (IU, PDF(($w''/<w''w''>^{1/2} \geq 2.3$) = 0.08). The tendency becomes more pronounced with increasing height. It is noteworthy that the pair of positive S_w (S_u) and K_w (K_u) ≥ 3 stimulate RSL vertical (streamwise) flow regime of SD and IU (SSD and ISA). For the remaining subzones, MSD and MU characterize the RSL flows. They diagnose negative and positive RSL skewness of vertical S_w and streamwise S_u velocities, respectively.

Apart from the noticeable downdraft above RSL of NO.9 induced by building heterogeneity, it is noted that, for $4H_a < z < 5H_a$ in NO.7, the modal vertical fluctuating velocity deviates much from its mean, signifying moderate downdraft ($-0.5 \leq w''/<w''w''>^{1/2} \leq -0.3$). It could be inferred that the substantial building heterogeneity ($K_h \geq 9$ and $\sigma_{Ha} \geq H_a$) and the maximum building height ($H_{max} \geq 4.4H_a$) would strengthen the downdraft. Such urban morphology could boost fresh air entrainment, improving pedestrian-level ventilation.

In spite of the dense buildings comparable to those in NO.7, moderate downdraft is merely observed in NO.2. More homogeneous-building predominant NO.2 could be the reason. This observation concurs the importance of building heterogeneity to RSL dynamics. With a slightly denser pattern, the vertical flows in NO.9 are more intermittent ($S_w > 0$ and $K_w > 3$) that triggers the extreme updraft. The urban morphology of NO.5 is similar to that of NO.9 but intermittent flow is not observed. As discussed in Sec.3.2, giant, upstream wakes could complicate the downstream flows in the subzones NO.5 and NO.2 so the roles of buildings in RSL turbulence generation are hardly differentiated. Further studies should consider how to separate the upstream wake effects, focusing on the dynamics attributed to the local buildings only. On the other hand, in the urban planning perspective, wakes after high-rise buildings should be considered before project development for sustainable cites.

3.6 Quadrant Analysis

To investigate the vertical transport mechanism of streamwise momentum, conditional sampling is conducted to partition the momentum flux $u''w''$ into four quadrants, i.e., $u''^{+}w''^{+}$ (Q1), $u''^{-}w''^{+}$ (Q2), $u''^{-}w''^{-}$ (Q3), and $u''^{+}w''^{-}$ (Q4), where the superscripts + and - denote a gain and a loss, respectively, relative to the mean velocities (Wallace & Brodkey 1977). The gradient events, ejection Q2 and sweep Q4, favor vertical momentum transport that strengthen the streamwise flows by either descending high-momentum winds (Q4) or bursting low-momentum winds (Q2). The time fraction

$$T_{Qi} = \frac{I_{Qi}}{\sum_{i=1}^{4} I_{Qi}} \tag{8}$$

is used to contrast the occurrence and the flux fraction

$$M_{Qi} = \frac{\langle u''w'' \rangle_{Qi}}{\sum_{i=1}^{4} \langle u''w'' \rangle_{Qi}} \quad (9)$$

the contribution. Here, the subscript Qi denotes the quadrant i and I_{Qi} is the number of events in the i^{th} quadrant.

Relationship between quadrants and flow statistics

The four quadrant events are organized into forward (streamwise accelerations Q1 and Q4) and backward (streamwise decelerations Q2 and Q3) motions (Guerrero et al., 2022). In RSL, majority flows decelerate ($-0.5 \le u''/\langle u''u''\rangle^{1/2} \le 0$; $T_{Q3} > T_{Q1}$ and $T_{Q2} > T_{Q4}$) while minority accelerate remarkably ($u''/\langle u''u''\rangle^{1/2} \ge 2.0$; $M_{Q4} > M_{Q2}$ and $M_{Q1} \approx M_{Q3}$; Figures 6). These findings concur the positive S_u discussed in Sections 3.3 and 3.4. Amid the subzones, Q2 occurs most frequently in NO.2 ($T_{Q2} \sim 35\%$) that signifies the highly skewed flows with intense, spur-like structures ($u''/\langle u''u''\rangle^{1/2} \ge 2.3$; Figure 5). This large portion of Q2 persists at higher elevation ($z \ge 5H_a$) in the subzones NO.2 and NO.5, lifting those decelerating air masses. The wakes behind high-rise buildings could extend a few kilometers horizontally (Inagaki et al., 2017) whose upper-level vortices ($z \ge 250$ m) could dominate the ejections (Park, Baik, & Han, 2015) or promote intermittent, extreme sweeps (Hertwig et al., 2017) at high elevation.

Among others, the RSL Q1 in NO.9 is apparently suppressed for $z \ge 2.2H_a$ ($T_{Q1} \le 15\%$) while its contribution remains unchanged ($M_{Q1} = -0.2$; Figure 6). Although its occurrence is comparable to that in other subzones, Q2 contributes substantially to momentum flux ($M_{Q2} \ge 0.4$). It is thus suggested that Q1 and Q2 consist of occasional, very strong vertical flows. With mild streamwise fluctuations (Figure 5a), fast, intermittent vertical flows are induced ($S_w \ge 0$ and $K_w \ge 3$), which, however, is not observed in other subzones. In our previous study [*Figure*

9 in Yao et al., (2022)], Q1 and Q3 are equally important to momentum transport (both time and flux fractions). On the contrary, with more diversified buildings, their occurrence is noticeably different.

In Sec. 3.3, it is also found that $S_u \geq 0$ and $S_w \geq 0$ around RSL top (the subzones NO.2, NO.5, and NO.6). It is especially profound in most RSL of NO.9. Likewise, the vertical fluctuating velocities are partitioned into updraft ($w'' > 0$; Q1 and Q2) and downdraft ($w'' < 0$; Q3 and Q4). At RSL top, it is notable that $T_{Q2} + T_{Q3} > T_{Q1} + T_{Q4}$ ($S_u > 0$) and $T_{Q3} + T_{Q4} > T_{Q1} + T_{Q2}$ ($S_w > 0$). It is logical to deduce that $T_{Q3} > T_{Q1}$. Therefore, outward events are more frequent than inward ones around RSL-ISL interface.

Roles of Q2 and Q4 in momentum transport

Approaching the roof level, downdraft hardly penetrates the UCL because of the physical blockage that degrades the entrainment efficiency. Under this circumstance, the anti-gradient (Q1 and Q3) and gradient (Q2 and Q4) events are comparable in terms of occurrence. With the increasing magnitude of momentum flux aloft, the gradient events (up to 71% in time at ISL top) play crucial roles in the transport. Especially, T_{Q2} is peaked around the drag center d (Figure 6) where the flows accelerate most (maximum S_u). This observation strengthens the role of ejections Q2 in low-level turbulence organization.

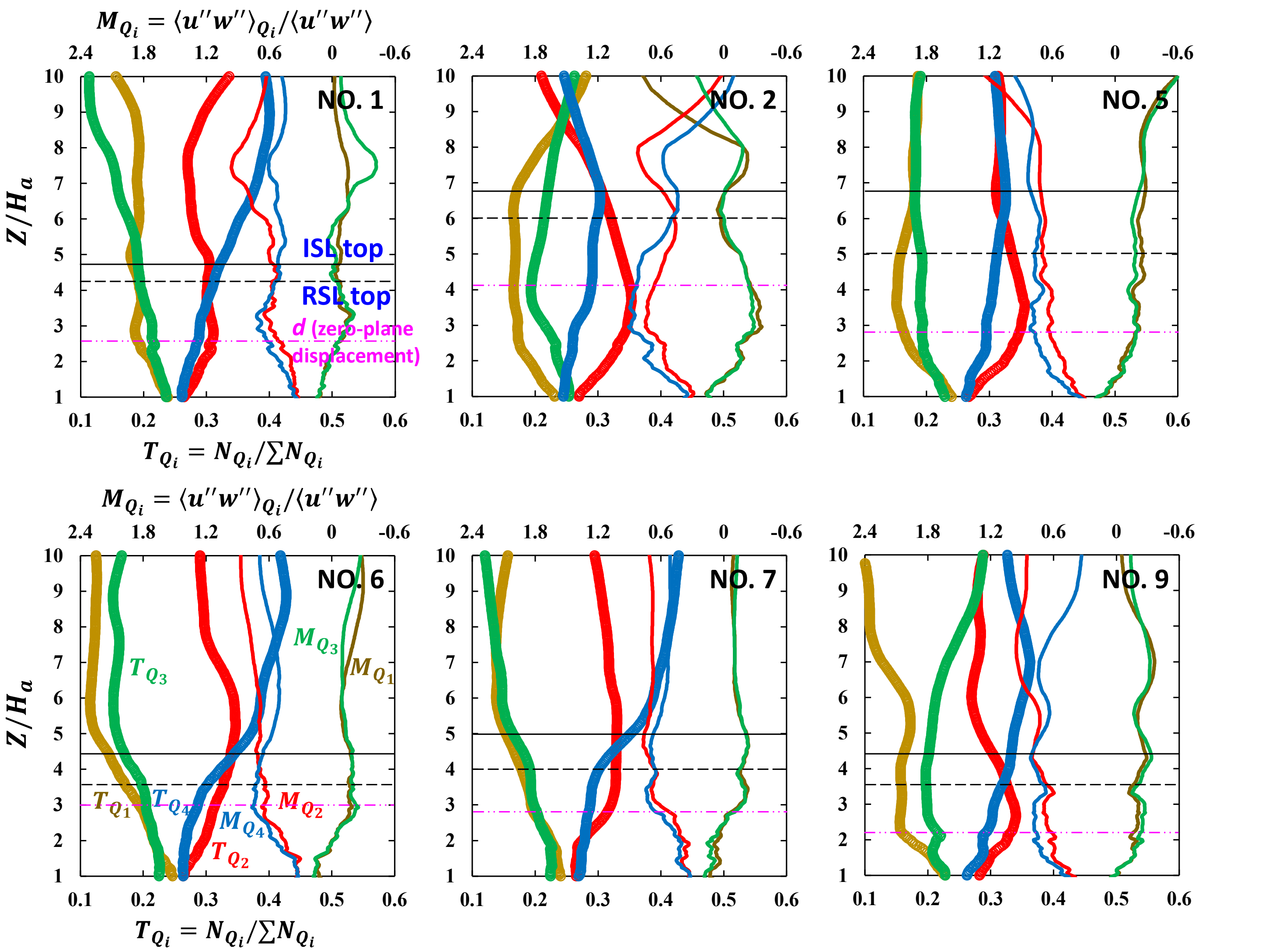

Figure 6. Time fraction T_{Qi} and momentum flux fraction M_{Qi} of individual quadrant events Q_i plotted as functions of height z/H_a.

460

Other than NO.2, it is interesting that T_{Q4} increases monotonically with increasing height throughout the ASLs. On the contrary, T_{Q2} develops a peak, mostly in the RSLs, then decreases thereafter (Figure 6). The reason could be the origin of rough-wall turbulence, i.e., the top-down or bottom-up theory (Li & Wang, 2018). The former states that TKE at lower level is provided by the (faster) freestream flows aloft. Whilst the latter supports the intrinsic turbulence structures being initiated by the surface-mounted roughness elements (Adrian, 2007). Their interaction was demonstrated by the energy increase (decrease) with height for low (high) wavenumber in pre-multiplied spectra (Wang & Zheng 2016). Hereby, Q4 entrains high-momentum fluids down to a low-momentum level whose occurrence reduces while approaching the ground (top-down theory). Whilst, Q2 accounts for detraining low-momentum fluid upwards to a high-momentum level within RSLs. It is thus tied with the surface-roughness-organized turbulence structures in the near-wall region (bottom-up theory).

Multiscale coherent structures and their relations to wakes and building morphology

To elucidate the effect of wakes and building heterogeneity, the occurrence of coherent structures from individual bins $T^*_{i,\eta}$ of filter size η (Yao et al., 2022) for subzones NO.5 and NO.9 are compared in Figure 7. These two subzones possess a similar building pattern in terms of $\lambda_p \approx 0.63$, $H_{max} \approx 88$ m, and $1 \leq \sigma_{Ha}/H_a \leq 1.1$ but the wakes upstream NO.5 are elongated. The results of other subzones are reported in Appendix (Figure A3). Within the RSLs, coherent structures appear less often with increasing strength. Especially at smaller η, say $\eta \approx 0.5$, Q2 appears more often ($T^*_{2,\eta} \approx 14\%$) than does Q4 ($T^*_{4,\eta} \approx 10\%$). Nonetheless, stronger Q4 occurs more frequently ($T^*_{4,\eta} \approx 2.6\%$, $T^*_{2,\eta} \approx 1.3\%$ for $\eta \geq 4.4$) whose overall contribution eventually outperforms its Q2 counterpart ($M_{Q4} > M_{Q2}$, Figure 6). Furthermore, the critical strength of turbulence structures to differentiate the dominance between Q2 and Q4 falls within the range of $3 \leq \eta \leq 5$ throughout the RSLs of all the subzones (Figure A4 in Appendix).

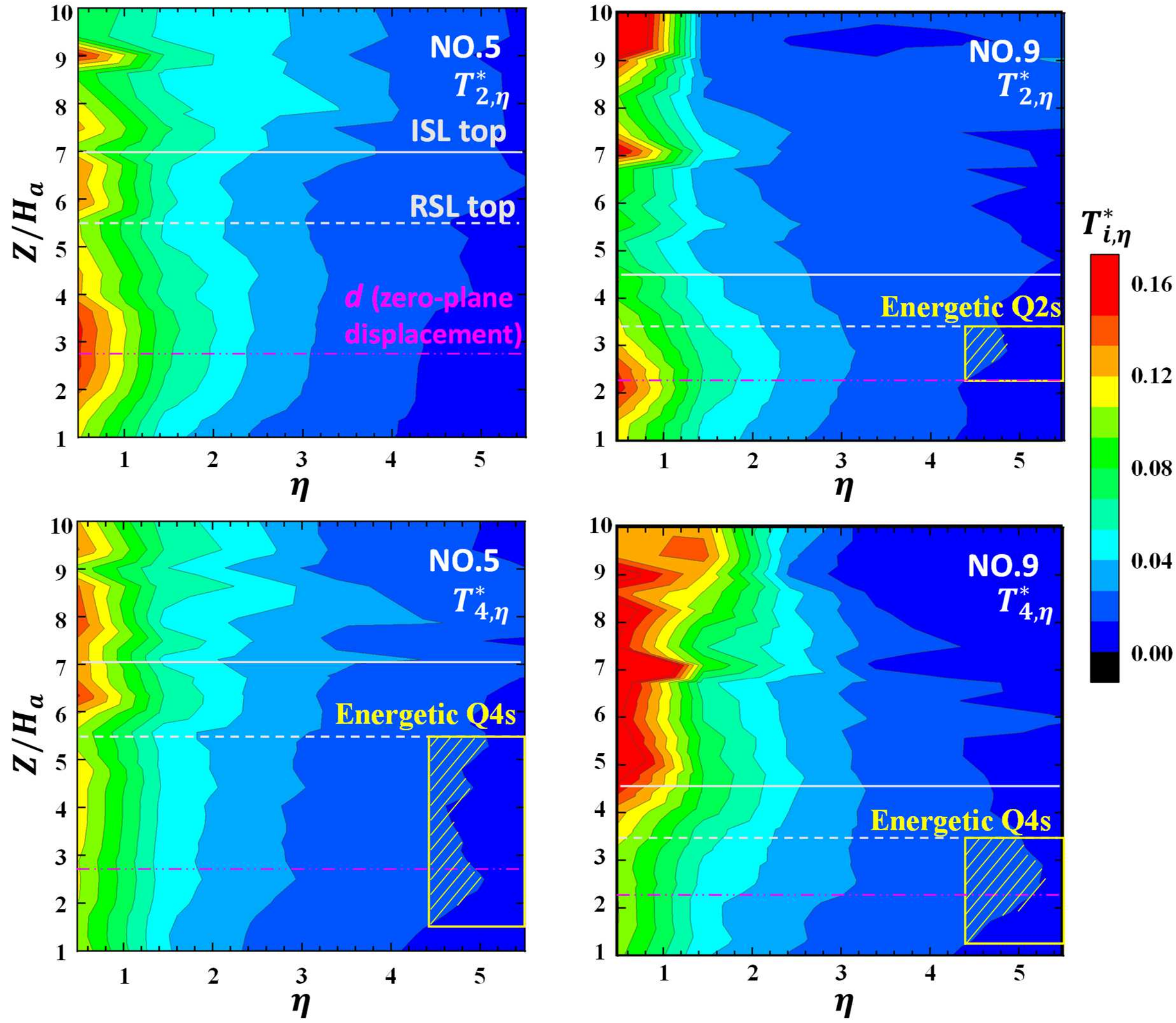

Figure 7. Shaded contours of time fraction of ejection $T^*_{2,\eta}$ and sweep $T^*_{4,\eta}$ plotted as functions of strength η and height z/H_a.

The energetic Q4 in NO.5 consists of strong streamwise acceleration ($u''/\langle u''u''\rangle^{1/2} \geq 2.3$), sustaining at elevated extent ($z \geq 5H_a$). Whereas, Q4 in NO.9 is composed of strong downdraft ($-0.7 \leq w''/\langle w''w''\rangle^{1/2} \leq 0$). In view of the strong updraft ($w''/\langle w''w''\rangle^{1/2} \geq 2.3$), intermittent, stronger Q2 are also embellished above $z \geq 2.2H_a$ in NO.9. These structures of energetic Q2 and Q4 are also observed in NO.7 with magnificent height heterogeneity. Moreover, strong Q4 is generated in NO.2 ($z \geq 3H_a$) in response to the upstream wake (Figure A3 in Appendix). Across all the cases, Q4 contributes mostly to the momentum flux despite its restrained occurrence (less than 30% in time; Figure 6). This finding suggests that upstream wakes could activate energetic Q4 to an extended ASL coverage in the vertical. It would promote the entrainment from the core to low-level winds. Building height variation stimulates both energetic Q2 and Q4, augmenting the vertical transport.

3.7 ASL Eddy Structure

Two-point correlation coefficient of streamwise velocity

$$R_{uu}\left(x_0, y_0, z_0; x, y, z\right) = \frac{\overline{u''\left(x_0, y_0, z_0\right) \times u''\left(x, y, z\right)}}{\left[\overline{u''\left(x_0, y_0, z_0\right) \times u''\left(x_0, y_0, z_0\right)}\right]^{1/2} \times \left[\overline{u''\left(x, y, z\right) \times u''\left(x, y, z\right)}\right]^{1/2}} \quad (10)$$

at the reference point (x_0, y_0, z_0) is used to depict the ASL turbulence structures (Coceal et al., 2007). Small-scale structures ($\approx 3H_a$) are initiated by the rather uniform buildings in NO.1 (Figure 8a) where the skimming flows dominate the transport over the dense buildings (Takimoto et al., 2013). On the other hand, at the center of NO.9 ($z = 2.8H_a$), large RSL turbulence structures (streamwise length scale $\approx 10H_a$) are generated by the heterogeneous buildings (Figure 8b) that are in line with those over schematic roughness (Wu & Christensen, 2007). The footprints of upstream wakes, which pass the center of NO.5, are identified by bulky upstream emanating contours ($R_{uu} \geq 0.9$; Figure 8c) whose size is almost $30H_a$ and an inclination angle $\Theta \approx 7^{\circ}$ throughout the ASL. These findings are consistent with those observed in near-neutral ASL (Marusic & Heuer, 2007). The invariant wake structure ($\Theta = 7^{\circ}$; Lee et al., 2011; Reynolds & Castro, 2008) further demonstrates the outer-layer similarity, supporting the top-down theory. The current inclination is comparable to that of smooth walls ($6^{\circ} \leq \Theta \leq 8^{\circ}$; Volino et al., 2007), wavy surfaces ($\Theta = 9^{\circ}$; Nakagawa & Hanratty, 2001), as well as ASLs ($\Theta \leq 10^{\circ}$; Heisel et al., 2018). Whereas, it is smaller than the range ($10^{\circ} \leq \Theta \leq 15^{\circ}$) reported by Liu *et al.* (2017) and Zhang *et al.* (2021) due to the weakened eddies and shear interfaces.

In the real-urban context, versatile turbulence structures are determined locally by the building morphology underneath (Salizzoni et al., 2011). In NO.5, there is a superposition of upstream steeply inclined ($13^{\mathrm{o}} \leq \Theta \leq 20^{\mathrm{o}}$) eddies ($R_{uu} \geq 0.9$) above a "step-up" building configuration (Figure 8c). A high-rise ($3H_a$), which is erected after another shorter building ($2H_a$), restricts the eddy extension downstream. However, a high-rise would steepen the eddy inclination ($\Theta \approx 19^{\mathrm{o}}$) right behind (NO.6, Figure A5 in Appendix). It is because, after separation at the building edges, the shear layer keeps thickening downstream, lifting the rear part of the eddies. Those peculiar shape, orientation, and size reflect the broad spectrum of multiscale eddies over cities, suggesting the diversified ASL turbulence structures in response to real urban morphology.

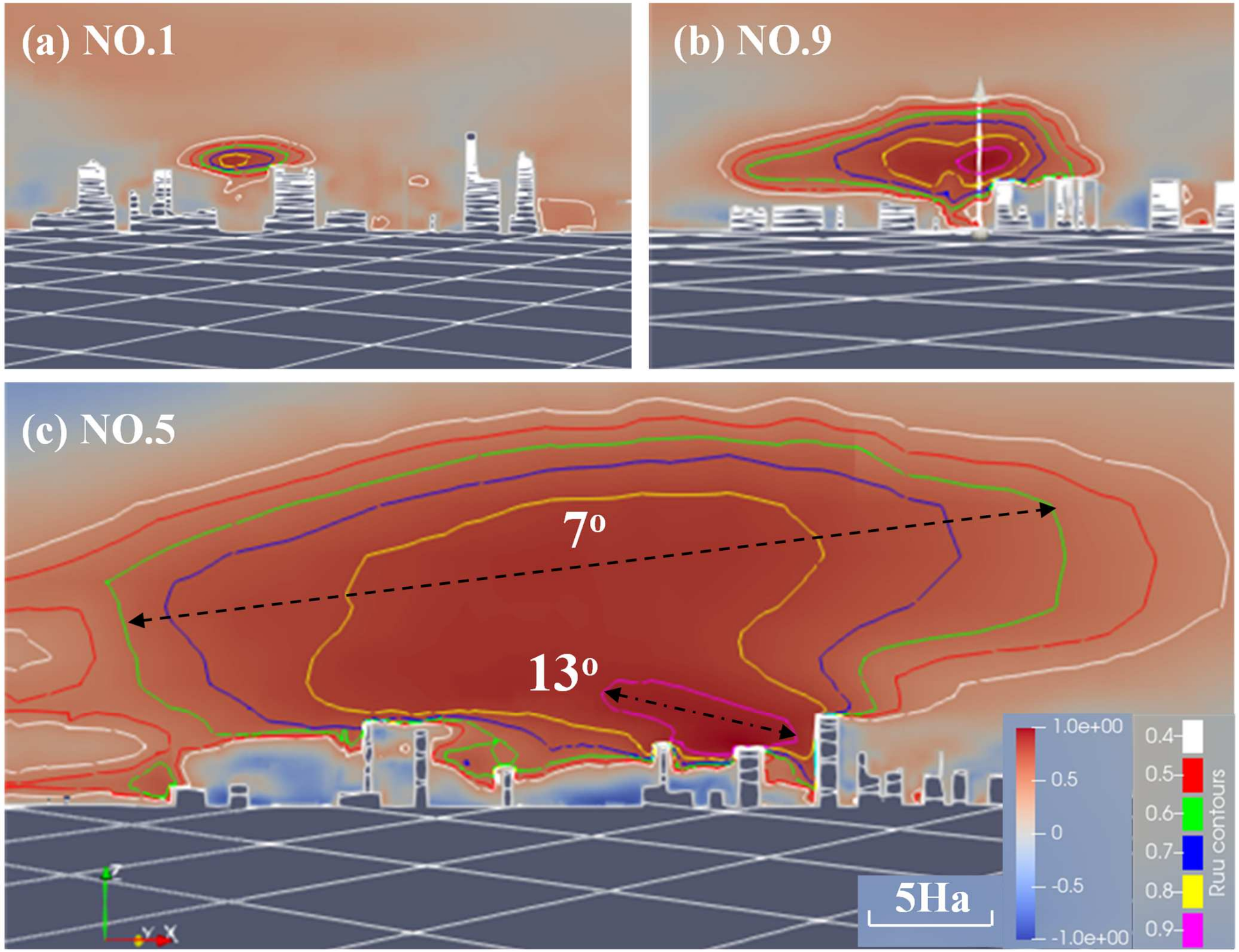

Figure 8. Shaded contours of two-point correlation coefficient of streamwise velocity R_{uu} at $z = 2.8H_a$ on x-z plane. Dark, dashed lines indicate the average inclination Θ and the characteristic length of the turbulence structures.

527

4. Discussion

The ASL flows over a real, dense urban area, Kowloon Peninsula, Hong Kong, are investigated by LESs in which buildings are explicitly resolved. In this paper, a comprehensive analytical method is applied to probe the turbulence dynamics in both ISLs and UCLs. The ASL flows are critically examined to reveal the highly non-Gaussian behaviors which are crucial to momentum transport and air quality (Khan et al., 2020). A dataset consisting of statistical indicators of turbulence (u_i'' and TKE) and structures (Q_i and eddies), together with the minority, majority and extreme flows (Su_i, Ku_i and PDF) is archived. Notably, the characteristic winds (Sec. 3.5) constitute the large-scale coherent structures which are diagnosed to examine the flow modification. The findings bridge the knowledge gap in the environmental fluid mechanics over heterogeneous (especially diversified, high-rise) buildings which is rather limited currently (Hertwig et al., 2021). Besides, the analytical methods, which uncover the physical processes of ASL turbulence over urban areas, have a broad impact on micrometeorological and geographical applications. This section elaborates the results obtained and the implications to urban planning guidelines.

The MWS profiles in ISLs are parameterized by the log-law. In this study, the physical significance of roughness length z_0 is verified as an indicator of surface roughness (measured by the friction velocity u_τ or the drag coefficient C_d). The zero-plane displacement d is in accordance with the maximum skewness of streamwise velocity S_u where the flows decelerate most. This finding evinces the role of d as a drag center in turbulence statistics. In view of the potential pollutant accumulation around d, where atmospheric flows decelerate most, it is helpful to formulate the guidelines for the height of local-scale building clusters so as to improve pedestrian-level air quality. Despite the assumptions behind the log-law over heterogeneous surfaces may not hold (Sützl et al., 2021), the results concur with the applicability of the conventional TBL theory over real, heterogeneous urban morphology. Moreover, incorporating the bulk aerodynamical indices (z_0, d, height of S_u peak) makes an urban climate model (UCM) rooted in the vigorous depiction of building-induced ASL momentum transport, enabling urban surface topologies adapted to climate change without solving the buildings explicitly in the planning.

The exp-law Equation (7), which is conducted on the UCL flows over real urban area unprecedentedly, predicting well the winds below d. Its characteristic being exerted by the real urban morphology leads to highly skewed streamwise ($S_u \geq 0$; MSD and ESA), and milder vertical flows ($S_w \leq 0$; MU and ED). By identifying Q2 and Q4 across a range of strength, a critical value of 3 to 5 times of the average momentum flux determines their dominance. The current MWS parameterizations and RSL dynamics contribute to a multilayer unified UCM in which the distinct UCL and ISL flows are resolved, enabling a sound, continuously tracking of airflows and pollutant transport at several vertical levels. Hence, facilities could be installed at designated locations for proper air quality monitoring. Since the wind field is generated across spatial heterogeneity, the multilayer model is more resilient than the single-layer one (Schoetter et al., 2020). Besides, the multilayer model could be used in the planning stage of development projects to estimate the ASL flows over diverse surface morphology (i.e., building layouts and configurations). It facilitates comprehensive datasets of the statistical, spatial wind distributions, offering quantitative evidence for policy innovation.

The response of dynamics on urban morphology provides insight for the arrangement of urban aggregations regarding the wakes generated by upstream clusters and local morphological factors (i.e., statistics of building height distribution). The extreme building height heterogeneity (H_{max}, K_h, and σ_{Ha}) promotes the intermittency of vertical winds ($S_w \geq 0$

and $K_w \geq 3$) for $z \geq 2H_a$, stimulating IU. It in turn helps forge energetic Q2 and Q4, augmenting the momentum transport. Upstream wake is conductive for RSL, raising the streamwise turbulence intensity. It lifts and amplifies small-scale Q2 in the decelerating region, rendering remarkable S_u ($\approx$ 0.7) to a large vertical extent and elevated drag center d. Although the intermittent streamwise winds ($K_u \geq 3$) are triggered where ISA takes place to form energetic Q4, residential areas should be avoided locating downstream bulky clusters to prevent from the drawback of massive, slow airflows with elevated pollutant levels. On the practical side, the annual average, dominant wind can be used to determine the prevailing wind in the planning stage of development projects. Note that dominant winds vary from city to city. Moreover, the wind statistics of the Kowloon Peninsula from 1998 to 2017 are given in the wind rose published elsewhere (Peng et al., 2018). On the other hand, building height variation is encouraged for improved street-level ventilation. Nevertheless, the excessive plan area density ($\lambda_p \sim 0.7$) should be avoided which is detrimental for momentum transport and turbulent mixing, restraining turbulence anisotropy. In particular, both Q2 and Q4 are mostly constrained in terms of occurrence and flux fraction in the RSLs of the densest subzone.

In real urban environment, the distribution of the upstream and local wakes is complex. In this study, the footprints of upstream wakes with certain size and inclination angle are identified by the contours of the two-point correlation R_{uu}, superimposing on the locally generated eddies. Local wakes collectively function as a streamwise envelope at the concerned points in the skimming-flow subzone. The two wakes interact that hardly distinguish the effects from neighborhood-scale buildings on the flows (see the length scales defined in Britter & Hanna, 2003). Besides, specific building arrangements could induce diversified eddies. Conspicuously, a high-rise building in the least heterogeneous case induces the most downstream inclined eddy right behind. Whilst, a combination of profound upstream wakes and a “step-up” structure triggers the largest upstream inclined eddy (R_{uu} = 0.9). In (or above) ISL, consistent inclination angles are found among the subzones. Generally, building heterogeneity is conductive to large, energetic eddy generation. While a more uniform, less building-covered surface forms smaller, less inclined turbulence structures. The eddies in building wakes govern local flow dynamics that is crucial to urban ventilation. Hence, urban-surface heterogeneity is favorable to vertical mixing and street-level ventilation by energetic eddies. Further investigation into local and non-local wakes could be developed.

5. Conclusion

ASL flows over a dense urban area are investigated. The applicability of the exp-law demonstrates a preliminary attempt on RSL-mean-flow parameterization. Compared with vegetation canopies and idealized roughness schemes, the mean winds over urban areas diminish faster, especially over specific morphological features, such as high plan area density, heterogeneous buildings. Statistically, the drag of ASL winds centers at the zero-plane displacement d that is in line with the elevation of maximum skewness of streamwise velocity.

Local urban morphology and upstream wakes are two key factors influencing flow dynamics and eddy formation. The imprints of upstream wakes are identified by persistent, bulky contours of two-point correlation R_{uu} throughout the ASL while the response to eddies above local buildings is depicted by distinctive shapes. Both building heterogeneity and upstream wakes could boost turbulence production and intermittent sweep structures ($-4.4\langle u''w''\rangle$), but excessive planar density ($\lambda_p \approx 0.7$) weakens. Building height variability could enhance the energy extraction from mean flows to vertical, leading to more occurrence of RSL SD and intermittent IU. Upstream wakes, however, could promote the streamwise fluctuating velocity, especially energizing ISA.

Coherent structures suggest the co-existence of top-down and bottom-up eddies. UBL flows demonstrate distinctive turbulence behaviors in response to real urban surfaces. With upstream wakes, elevated region of frequent Q2 leads to large, positive S_u and notable $K_u \geq 3$. While in the most heterogeneous case (NO.9), Q1 is substantially suppressed, provoking $K_w \geq 3$. The results show the superiority of height heterogeneity in large-eddy generation which is beneficial to vertical transport. The current depiction would contribute to supplement wall-models as well as advance the understanding of ASL winds over real, dense cities. The outcome in turn helps improve the air quality by proper urban planning.

Acknowledgements

This research is conducted in part using the research computing facilities and/or advisory services offered by Information Technology Services (ITS), The University of Hong Kong (HKU). Technical support from Ms. Lilian Y.L. Chan, Mr. W.K. Kwan, Mr. Bill H.T. Yau, and Mr. Juilian Yeung is appreciated. This study is partly supported by the Hong Kong (HK) Research Grants Council (RGC) Theme-based Research Scheme (TRS) T24-504/17-N, the HK RGC Collaborative Research Fund (CRF) C7064 18G and C5108 20G, as well as the HK RGC General Research Fund (GRF) 17209819 and 17211322. The authors are very thankful to the constructive comment raised by the two anonymous reviewers. The insightful reviews are detailed and helpful to improve the manuscript.

Appendix

Supplementary dataset to this article is attached as a separate file.

References

Adrian, R. J. (2007). Hairpin vortex organization in wall turbulence. *Physics of Fluids*, *19*(4), 041301. https://doi.org/10.1063/1.2717527

Adrian, R. J., Meinhart, C. D., & Tomkins, C. D., (2000). Vortex organization in the outer region of the turbulent boundary layer. *Journal of fluid Mechanics*, *422*, 1-54. https://doi.org/10.1017/s0022112000001580

Apsilidis, N., Diplas, P., Dancey, C. L., & Bouratsis, P. (2015). Time-resolved flow dynamics and Reynolds number effects at a wall-cylinder junction. *Journal of Fluid Mechanics*, *776*, 475-511. https://doi.org/10.1017/jfm.2015.341

Böhm, M., Finnigan, J. J., Raupach, M. R., & Hughes, D. (2013). Turbulence structure within and above a canopy of bluff elements. *Boundary-Layer Meteorology*, *146*, 393-419. https://doi.org/10.1007/s10546-012-9770-1

Britter, R. E., & Hanna, S. R. (2003). Flow and dispersion in urban areas. *Annual Review of Fluid Mechanics*, *35*(1), 469-496. https://doi.org/10.1146/annurev.fluid.35.101101.161147

Byrne, R., Hewitt, N. J., Griffiths, P., & MacArtain, P. (2021). A comparison of four microscale wind flow models in predicting the real-world performance of a large-scale peri-urban wind turbine, using onsite LiDAR wind measurements. *Sustainable Energy Technologies and Assessments*, *46*, 101323. https://doi.org/10.1016/j.seta.2021.101323

Capolongo, S., Rebecchi, A., Buffoli, M., Appolloni, L., Signorelli, C., Fara, G.M., & D'Alessandro, D. (2020). COVID-19 and cities: From urban health strategies to the pandemic challenge. A decalogue of public health opportunities. *Acta Bio Medica: Atenei Parmensis*, *91*(2), 13.

Castro, I. P. (2017). Are urban-canopy velocity profiles exponential? *Boundary-Layer Meteorology*, *164*(3), 337-351. https://doi.org/10.1007/s10546-017-0258-x

Chen, Q., Qi, M., Zhong, Q., & Li, D. (2017). Experimental study on the multimodal dynamics of the turbulent horseshoe vortex system around a circular cylinder. *Physics of Fluids*, *29*(1), 015106. https://doi.org/10.1063/1.4974523

Cheng, H., & Castro, I. P. (2002). Near wall flow over urban-like roughness. *Boundary-Layer Meteorology*, *104*, 229-259. https://doi.org/10.1023/A:1016060103448

Cheng, W. C., Liu, C.-H., Ho, Y.-K., Mo, Z., Wu, Z., Li, W., Chan, L. Y. L., Kwan, W. K., & Yau, H. T. (2021). Turbulent flows over real heterogeneous urban surfaces: Wind tunnel experiments and Reynolds-averaged Navier-Stokes simulations. *Building Simulation*, *14*,1345-1358. https://doi.org/10.1007/s12273-020-0749-4

Cheng, W.C., & Yang, Y. (2022). Scaling of flows over realistic urban geometries: a large-eddy simulation study. *Boundary-Layer Meteorology*, *186*(1), 125-144. https://doi.org/10.1007/s10546-022-00749-y

Cionco, R. M. (1965). A mathematical model for air flow in a vegetative canopy. *Journal of Applied Meteorology and Climatology*, *4*(4), 517-522. https://doi.org/10.1175/1520-0450(1965)004<0517:ammfaf>2.0.co;2

Coceal, O., Dobre, A., Thomas, T. G., & Belcher, S. E. (2007). Structure of turbulent flow over regular arrays of cubical roughness. *Journal of Fluid Mechanics*, *589*, 375-409. https://doi.org/10.1017/S002211200700794X

Coceal, O., Thomas, T. G., Castro, I. P., & Belcher, S. E. (2006). Mean flow and turbulence statistics over groups of urban-like cubical obstacles. *Boundary-Layer Meteorology*, *121*, 491-519. https://doi.org/10.1007/s10546-006-9076-2

Drobinski, P., Carlotti, P., Newsom, R. K., Banta, R. M., Foster, R. C., & Redelsperger, J. L. (2004). The structure of the near-neutral atmospheric surface layer. *Journal of the Atmospheric Sciences*, *61*(6), 699-714. https://doi.org/10.1175/1520-0469(2004)061<0699:TSOTNA>2.0.CO;2

Duan, G., & Takemi, T. (2021). Gustiness in thermally-stratified urban turbulent boundary-layer flows and the influence of surface roughness. *Journal of Wind Engineering and Industrial Aerodynamics*, *208*, 104442. https://doi.org/10.1016/j.jweia.2020.104442

Elbing, B. R., Solomon, M. J., Perlin, M., Dowling, D. R., & Ceccio, S. L. (2011). Flow-induced degradation of drag-reducing polymer solutions within a high-Reynolds-number turbulent boundary layer. *Journal of Fluid Mechanics*, *670*, 337-364. https://doi.org/10.1017/S0022112010005331

Furtak-Cole, E., & Ngan, K. (2020). Predicting mean velocity profiles inside urban canyons. *Journal of Wind Engineering and Industrial Aerodynamics*, *207*, 104280. https://doi.org/10.1016/j.jweia.2020.104280

García-Sánchez, C., van Beeck, J., & Gorlé, C., (2018). Predictive large eddy simulations for urban flows: Challenges and opportunities. *Building and Environment*, *139*, 146-156. https://doi.org/10.1016/j.buildenv.2018.05.007

Giometto, M. G., Christen, A., Meneveau, C., Fang, J., Krafczyk, M., & Parlange, M. B. (2016). Spatial characteristics of roughness sublayer mean flow and turbulence over a realistic urban surface. *Boundary-Layer Meteorology*, *160*. 425-452. https://doi.org/10.1007/s10546-016-0157-6

Guerrero, B., Lambert, M. F., & Chin, R. C. (2022). Precursors of backflow events and their relationship with the near-wall self-sustaining process. *Journal of Fluid Mechanics*, *933*, A33. https://doi.org/10.1017/jfm.2021.1082

Guo, L., Luo, J., Yuan, M., Huang, Y., Shen, H. & Li, T. (2019). The influence of urban planning factors on PM2. 5 pollution exposure and implications: A case study in China based on remote sensing, LBS, and GIS data. *Science of The Total Environment*, *659*, 1585-1596. https://doi.org/10.1016/j.scitotenv.2018.12.448

Hagishima, A., Tanimoto, J., Nagayama, K., & Meno, S. (2009). Aerodynamic parameters of regular arrays of rectangular blocks with various geometries. *Boundary-Layer Meteorology*, *132*, 315-337. https://doi.org/10.1007/s10546-009-9403-5

Han, B. S., Park, S. B., Baik, J. J., Park, J., & Kwak, K. H. (2017). Large-eddy simulation of vortex streets and pollutant dispersion behind high-rise buildings. *Quarterly Journal of the Royal Meteorological Society*, *143*(708), 2714-2726. https://doi.org/10.1002/qj.3120

Harman I. N., & Finnigan J. J. (2007). A simple unified theory for flow in the canopy and roughness sublayer. *Boundary-Layer Meteorology*, *123*, 339-363. https://doi.org/10.1007/s10546-006-9145-6

Hayati, A. N., Stoll, R., Pardyjak, E. R., Harman, T., & Kim, J. J. (2019). Comparative metrics for computational approaches in non-uniform street-canyon flows. *Building and Environment*, *158*, 16-27. https://doi.org/10.1016/j.buildenv.2019.04.028

He, B. J., Ding, L., & Prasad, D. (2019). Enhancing urban ventilation performance through the development of precinct ventilation zones: A case study based on the Greater Sydney, Australia. *Sustainable Cities and Society*, *47*, 101472. https://doi.org/10.1016/j.scs.2019.101472

Heisel, M., Dasari, T., Liu, Y., Hong, J., Coletti, F., & Guala, M. (2018). The spatial structure of the logarithmic region in very-high-Reynolds-number rough wall turbulent boundary layers. *Journal of Fluid Mechanics*, *857*, 704-747. https://doi.org/10.1017/jfm.2018.759

Hertwig, D., Gough, H. L., Grimmond, S., Barlow, J. F., Kent, C. W., Lin, W. E., Robins, A. G., & Hayden, P. (2019). Wake characteristics of tall buildings in a realistic urban canopy. *Boundary-Layer Meteorology*, *172*(2), 239-270. https://doi.org/10.1007/s10546-019-00450-7

Hertwig, D., Grimmond, S., Kotthaus, S., Vanderwel, C., Gough, H., Haeffelin, M., & Robins, A. (2021). Variability of physical meteorology in urban areas at different scales: Implications for air quality. *Faraday Discussions*, *226*, 149-172. https://doi.org/10.1039/d0fd00098a

Hertwig, D., Patnaik, G., & Leitl, B. (2017). LES validation of urban flow, part II: eddy statistics and flow structures. *Environmental Fluid Mechanics*, *17*, 551-578. https://doi.org/10.1007/s10652-016-9504-x

Ho, Y.-K., & Liu, C.-H. (2017). A wind tunnel study of flows over idealised urban surfaces with roughness sublayer corrections. *Theoretical and Applied Climatology, 130*, 305-320. https://doi.org/10.1007/s00704-016-1877-8

Huang, X., Gao, L., Guo, D., & Yao, R. (2021). Impacts of high-rise building on urban airflows and pollutant dispersion under different temperature stratifications: Numerical investigations. *Atmospheric Pollution Research, 12*(3), 100-112. https://doi.org/10.1016/j.apr.2021.02.001

Inagaki, A., Kanda, M., Ahmad, N. H., Yagi, A., Onodera, N., & Aoki, T. (2017). A numerical study of turbulence statistics and the structure of a spatially-developing boundary layer over a realistic urban geometry. *Boundary-Layer Meteorology*, *164*, 161-181. https://doi.org/10.1007/s10546-017-0249-y

Jiang, D., Jiang, W., Liu, H., & Sun, J. (2008). Systematic influence of different building spacing, height and layout on mean wind and turbulent characteristics within and over urban building arrays. *Wind and Structures, An International Journal*, *11*(4), 275-290. https://doi.org/10.12989/was.2008.11.4.275

Kanda, M., Inagaki, A., Miyamoto, T., Gryschka, M., & Raasch, S. (2013). A new aerodynamic parametrization for real urban surfaces. *Boundary-Layer Meteorology, 148*(2), 357-377. https://doi.org/10.1007/s10546-013-9818-x

Khan, S. &Hassan, Q. (2020). Review of developments in air quality modelling and air quality dispersion models. *Journal of Environmental Engineering and Science*, *16*(1), 1-10.

Lee, J. H., Sung, H. J., & Krogstad, P. Å. (2011). Direct numerical simulation of the turbulent boundary layer over a cube-roughened wall. *Journal of Fluid Mechanics*, *669*, 397-431. https://doi.org/10.1017/S0022112010005082

Leonardi, S., & Castro, I. P. (2010). Channel flow over large cube roughness: A direct numerical simulation study. *Journal of Fluid Mechanics*, *651*, 519-539. https://doi.org/10.1017/S002211200999423X

Letzel, M. O., Helmke, C., Ng, E., An, X., Lai, A., & Raasch, S. (2012). LES case study on pedestrian level ventilation in two neighbourhoods in Hong Kong. *Meteorologische Zeitschrift*, *21*(6), 575-589. https://doi.org/10.1127/0941-2948/2012/0356

Li, J., You, W. & Ding, W. (2022). Exploring urban space quantitative indicators associated with outdoor ventilation potential. *Sustainable Cities and Society*, *79*, 103696. https://doi.org/10.1016/j.scs.2022.103696

Li, Q., & Bou-Zeid, E. (2019). Contrasts between momentum and scalar transport over very rough surfaces. *Journal of Fluid Mechanics*, *880*, 32-58. https://doi.org/10.1017/jfm.2019.687

Li, Q., & Katul, G. (2022). Bridging the urban canopy sublayer to aerodynamic parameters of the atmospheric surface layer. *Boundary-Layer Meteorology*, *185*(1), 35-61. https://doi.org/10.1007/s10546-022-00723-8

Li, Q., & Wang, Z. H. (2018). Large-eddy simulation of the impact of urban trees on momentum and heat fluxes. *Agricultural and Forest Meteorology*, *255*, 44-56. https://doi.org/10.1016/j.agrformet.2017.07.011

Li, X. X., Liu, C. H., & Leung, D. Y. C. (2008). Large-eddy simulation of flow and pollutant dispersion in high-aspect-ratio urban street canyons with wall model. *Boundary-Layer Meteorology*, *129*, 249-268. https://doi.org/10.1007/s10546-008-9313-y

Li, Z., Ming, T., Liu, S., Peng, C., de Richter, R., Li, W., Zhang, H., & Wen, C. Y. (2021). Review on pollutant dispersion in urban areas-part A: Effects of mechanical factors and urban morphology. *Building and Environment*, *190*, 107534. https://doi.org/10.1016/j.buildenv.2020.107534

Lim, H. D., Hertwig, D., Grylls, T., Gough, H., Reeuwijk, M.V., Grimmond, S., & Vanderwel, C. (2022). Pollutant dispersion by tall buildings: Laboratory experiments and large-eddy simulation. *Experiments in Fluids*, *63*(6), 92. https://doi.org/10.1007/s00348-022-03439-0

Liu, H. Y., Bo, T. L., & Liang, Y. R. (2017). The variation of large-scale structure inclination angles in high Reynolds number atmospheric surface layers. *Physics of Fluids*, *29*(3), 035104. https://doi.org/10.1063/1.4978803

Liu, S., Kwok, Y. T. & Ren, C. (2023). Investigating the impact of urban microclimate on building thermal performance: a case study of dense urban areas in Hong Kong. *Sustainable Cities and Society*, *94*, 104509. https://doi.org/10.1016/j.scs.2023.104509

Luhar, M., Rominger, J., & Nepf, H. (2008). Interaction between flow, transport and vegetation spatial structure. *Environmental Fluid Mechanics*, *8*, 423-439. https://doi.org/10.1007/s10652-008-9080-9

Marusic, I., & Heuer, W. D. C. (2007). Reynolds number invariance of the structure inclination angle in wall turbulence. *Physical Review Letters*, *99*(11), 114504. https://doi.org/10.1103/PhysRevLett.99.114504

Miao, Y., Liu, S., Zheng, Y., Wang, S., & Li, Y. (2014). Numerical study of traffic pollutant dispersion within different street canyon configurations. *Advances in Meteorology*, *2014*. https://doi.org/10.1155/2014/458671

Mo, Z., Liu, C.-H., & Ho, Y.-K. (2021). Roughness sublayer flows over real urban morphology: A wind tunnel study. *Building and Environment*, *188*, 107463. https://doi.org/10.1016/j.buildenv.2020.107463

Mo, Z., & Liu, C.-H. (2023). Inertial and roughness sublayer flows over real urban morphology: A comparison of wind tunnel experiment and large-eddy simulation. *Urban Climate, 49*, 101530. https://doi.org/10.1016/j.uclim.2023.101530

Nakagawa, S., & Hanratty, T. J. (2001). Particle image velocimetry measurements of flow over a wavy wall. *Physics of Fluids*, *13*(11), 3504-3507. https://doi.org/10.1063/1.1399291

Oke, T. R. (1988). Street design and urban canopy layer climate. *Energy and Buildings*, *11*(1-3), 103-113. https://doi.org/10.1016/0378-7788(88)90026-6

Palusci, O., Monti, P., Cecere, C., Montazeri, H. & Blocken, B. (2022). Impact of morphological parameters on urban ventilation in compact cities: The case of the Tuscolano-Don Bosco district in Rome. *Science of the Total Environment*, *807*, 150490. https://doi.org/10.1016/j.scitotenv.2021.150490

Papp, B., Kristóf, G., Istók, B., Koren, M., Balczó, M., & Balogh, M. (2021). Measurement-driven large eddy simulation of dispersion in street canyons of variable building height. *Journal of Wind Engineering and Industrial Aerodynamics*, *211*, 104495. https://doi.org/10.1016/j.jweia.2020.104495

Park, S. B., Baik, J. J., & Han, B. S. (2015). Large-eddy simulation of turbulent flow in a densely built-up urban area. *Environmental Fluid Mechanics*, *15*, 235-250. https://doi.org/10.1007/s10652-013-9306-3

Park, S. B., Baik, J. J., & Lee, S. H. (2015). Impacts of mesoscale wind on turbulent flow and ventilation in a densely built-up urban area. *Journal of Applied Meteorology and Climatology*, *54*(4), 811-824. https://doi.org/10.1175/JAMC-D-14-0044.1

Peng, L., Liu, J.P., Wang, Y., Chan, P.W., Lee, T.C., Peng, F., Wong, M.S. & Li, Y. (2018). Wind weakening in a dense high-rise city due to over nearly five decades of urbanization. *Building and Environment*, *138*, 207-220.

Peterka, J. A., Meroney, R. N., & Kothari, K. M. (1985). Wind flow patterns about buildings. *Journal of Wind Engineering and Industrial Aerodynamics*, *21*(1), 21-38. https://doi.org/10.1016/0167-6105(85)90031-5

Ramirez, N., Afshari, A., & Norford, L. (2018). Validation of simplified urban-canopy aerodynamic parametrizations using a numerical simulation of an actual downtown area. *Boundary-Layer Meteorology*, *168*, 155-187. https://doi.org/10.1007/s10546-018-0345-7

Ratti, C., Di Sabatino, S., Britter, R., Brown, M., Caton, F., & Burian, S. (2002). Analysis of 3-D urban databases with respect to pollution dispersion for a number of European and American cities. *Water, Air and Soil Pollution: Focus* *2*, 459-469. https://doi.org/10.1007/978-94-010-0312-4_33

Reynolds, R. T., & Castro, I. P. (2008). Measurements in an urban-type boundary layer. *Experiments in Fluids*, *45*, 141-156. https://doi.org/10.1007/s00348-008-0470-z

Sabatino, S.D., Barbano, F., Brattich, E. & Pulvirenti, B. (2020). The multiple-scale nature of urban heat island and its footprint on air quality in real urban environment. *Atmosphere*, *11*(11), 1186.

Salizzoni, P., Marro, M., Soulhac, L., Grosjean, N., & Perkins, R. J. (2011). Turbulent Transfer Between Street Canyons and the Overlying Atmospheric Boundary Layer. *Boundary-Layer Meteorology*, *141*(3), 393-414. https://doi.org/10.1007/s10546-011-9641-1

Santiago, J. L., & Martilli, A. (2010). A Dynamic Urban Canopy Parameterization for Mesoscale Models Based on Computational Fluid Dynamics Reynolds-Averaged Navier-Stokes Microscale Simulations. *Boundary-Layer Meteorology*, *137*, 417-439. https://doi.org/10.1007/s10546-010-9538-4

Schanderl, W., Jenssen, U., Strobl, C., & Manhart, M. (2017). The structure and budget of turbulent kinetic energy in front of a wall-mounted cylinder. *Journal of Fluid Mechanics*, *827*, 285-321. https://doi.org/10.1017/jfm.2017.486

Schoetter, R., Kwok, Y.T., de Munck, C., Lau, K.K.L., Wong, W.K. & Masson, V. (2020). Multi-layer coupling between SURFEX-TEB-v9. 0 and Meso-NH-v5. 3 for modelling the urban climate of high-rise cities. *Geoscientific Model Development*, *13*(11), 5609-5643.

Smagorinsky, J. (1963). General circulation experiments with the primitive equations: I. The basic experiment. *Monthly Weather Review*, *91*(3), 99-164. https://doi.org/10.1175/1520-0493(1963)091<0099:gcewtp>2.3.co;2

Sützl, B. S., Rooney, G. G., & van Reeuwijk, M. (2020). Drag distribution in idealized heterogeneous urban environments. *Boundary-Layer Meteorology*, *178*(2), 225-248. https://doi.org/10.1007/s10546-020-00567-0

Sützl, B.S., Rooney, G.G., Finnenkoetter, A., Bohnenstengel, S.I., Grimmond, S., & van Reeuwijk, M. (2021). Distributed urban drag parametrization for sub-kilometre scale numerical weather prediction. *Quarterly Journal of the Royal Meteorological Society*, *147*(741), 3940-3956.

Takimoto, H., Inagaki, A., Kanda, M., Sato, A., & Michioka, T. (2013). Length-scale similarity of turbulent organized structures over surfaces with different roughness types. *Boundary-Layer Meteorology*, *147*, 217-236. https://doi.org/10.1007/s10546-012-9790-x

Volino, R. J., Schultz, M. P., & Flack, K. A. (2007). Turbulence structure in rough- and smooth-wall boundary layers. *Journal of Fluid Mechanics*, *592*, 263-293. https://doi.org/10.1017/S0022112007008518

Wallace, J. M., & Brodkey, R. S. (1977). Reynolds stress and joint probability density distributions in the u-v plane of a turbulent channel flow. *Physics of Fluids*, *20*(3), 351-355. https://doi.org/10.1063/1.861897

Wang, G., & Zheng, X. (2016). Very large scale motions in the atmospheric surface layer: a field investigation. *Journal of Fluid Mechanics*, *802*, 464-489. https://doi.org/10.1017/JFM.2016.439

Wu, Y., & Christensen, K. T. (2007). Outer-layer similarity in the presence of a practical rough-wall topography. *Physics of Fluids*, *19*(8), 085108. https://doi.org/10.1063/1.2741256

Xie, Z. T., Coceal, O., & Castro, I. P. (2008). Large-eddy simulation of flows over random urban-like obstacles. *Boundary-Layer Meteorology*, *129*, 1-23. https://doi.org/10.1007/s10546-008-9290-1f

Xu, F. & Gao, Z. (2022). Frontal area index: A review of calculation methods and application in the urban environment. *Building and Environment*, 109588.

Yakhot, A., Liu, H., & Nikitin, N. (2006). Turbulent flow around a wall-mounted cube: A direct numerical simulation. *International Journal of Heat and Fluid Flow*, *27*(6), 994-1009. https://doi.org/10.1016/j.ijheatfluidflow.2006.02.026

Yang, X. I. A., Sadique, J., Mittal, R., & Meneveau, C. (2016). Exponential roughness layer and analytical model for turbulent boundary layer flow over rectangular-prism roughness elements. *Journal of Fluid Mechanics*, *789*, 127-165. https://doi.org/10.1017/jfm.2015.687

Yao, L., Liu, C.-H., Mo, Z., Cheng, W. C., Brasseur, G. P., & Chao, C. Y. H. (2022). Statistical analysis of the organized turbulence structure in the inertial and roughness sublayers over real urban area by building-resolved large-eddy simulation. *Building and Environment*, *207*, 108464. https://doi.org/10.1016/j.buildenv.2021.108464

Yoshida, T., Takemi, T. & Horiguchi, M. (2018). Large-eddy-simulation study of the effects of building-height variability on turbulent flows over an actual urban area. *Boundary-Layer Meteorology*, *168*, 127-153.

Yuan, C., Shan, R., Zhang, Y., Li, X.X., Yin, T., Hang, J. & Norford, L. (2019). Multilayer urban canopy modelling and mapping for traffic pollutant dispersion at high density urban areas. *Science of the total environment*, *647*, 255-267. https://doi.org/10.1016/j.scitotenv.2018.07.409

Zhang, W., Wan, M., Xia, Z., Wang, J., Lu, X., & Chen, S. (2021). Constrained large-eddy simulation of turbulent flow over rough walls. *Physical Review Fluids*, *6*(4), 044602. https://doi.org/10.1103/PhysRevFluids.6.044602

Zhao, Y., Li, H., Kubilay, A. & Carmeliet, J. (2021). Buoyancy effects on the flows around flat and steep street canyons in simplified urban settings subject to a neutral approaching boundary layer: Wind tunnel PIV measurements. *Science of the Total Environment*, *797*, 149067. https://doi.org/10.1016/j.scitotenv.2021.149067

Zhu, X., Iungo, G. V., Leonardi, S., & Anderson, W. (2017). Parametric study of urban-like topographic statistical moments relevant to a priori modelling of bulk aerodynamic parameters. *Boundary-Layer Meteorology*, *162*(2), 231-253. https://doi.org/10.1007/s10546-016-0198-x